1 **A mosaic of phytoplankton responses across Patagonia, the southeast Pacific and**

2 **southwest Atlantic Oceans to ash deposition and trace metal release from the Calbuco**

3 **volcanic eruption in 2015**

4 Maximiliano J. Vergara-Jara[1,2], Mark J. Hopwood[3*], Thomas J. Browning[3], Insa Rapp[4],

5 Rodrigo Torres[2,5], Brian Reid[5], Eric P. Achterberg[3], José Luis Iriarte[2,6].

6

7 [1]Programa de Doctorado en Ciencias de la Acuicultura, Universidad Austral de Chile, Puerto

8 Montt, Chile.

9 [2]Instituto de Acuicultura & Centro de Investigación Dinámica de Ecosistemas Marinos de

10 Altas Latitudes - IDEAL, Universidad Austral de Chile, Puerto Montt, Chile.

11 [3]GEOMAR, Helmholtz Centre for Ocean Research, 24148 Kiel, Germany.

12 [4]Department of Biology, Dalhousie University, Halifax, Nova Scotia, Canada

13 [5]Centro de Investigación en Ecosistemas de la Patagonia (CIEP), Coyhaique, Chile.

14 [6]COPAS-Sur Austral, Centro de Investigación Oceanográfica en el Pacífico Sur-Oriental

15 (COPAS), Universidad de Concepción, Concepción, Chile.

16
17 Key words: volcanic ash, iron, Fe(II), phytoplankton, carbonate chemistry, Reloncaví Fjord

18 Corresponding author*: mhopwood@geomar.de
19
20
21
22
23
24
25
26
27
28
29
30
31
32
33
34
35
36
37

Abstract

Following the eruption of the Calbuco volcano in April 2015, an extensive ash plume spread across northern Patagonia and into the southeast Pacific and southwest Atlantic Oceans. Here we report on field surveys conducted in the coastal region receiving the highest ash load following the eruption (Reloncaví Fjord). The fortuitous location of a long-term monitoring station in Reloncaví Fjord provided data to evaluate inshore phytoplankton bloom dynamics and carbonate chemistry during April-May 2015. Satellite derived chlorophyll-a measurements over the ocean regions affected by the ash plume in May 2015 were obtained to determine the spatial-temporal gradients in offshore phytoplankton response to ash. Additionally, leaching experiments were performed to quantify the release from ash into solution of total alkalinity, trace elements (dissolved Fe, Mn, Pb, Co, Cu, Ni and Cd) and major ions (F^-, Cl^-, SO_4^{2-}, NO_3^-, Li^+, Na^+, NH_4^+, K^+, Mg^{2+}, Ca^{2+}). Within Reloncaví Fjord, integrated peak diatom abundances during the May 2015 austral bloom were approximately 2-4 times higher than usual (up to 1.4×10^{11} cells m^{-2}, integrated to 15 m depth), with the bloom intensity perhaps moderated due to high ash loadings in the two weeks following the eruption. Any mechanistic link between ash deposition and the Reloncaví diatom bloom can however only be speculated on due to the lack of data immediately preceding and following the eruption. In the offshore southeast Pacific, a short duration phytoplankton bloom corresponded closely in space and time to the maximum observed ash plume, potentially in response to Fe-fertilization of a region where phytoplankton growth is typically Fe-limited at this time of year. Conversely, no clear fertilization on the same time-scale was found in the area subject to an ash plume over the southwest Atlantic where the availability of fixed nitrogen is thought to limit phytoplankton growth. This was consistent with no significant release of fixed nitrogen (NO_x or NH_4) from Calbuco ash.

62

63   In addition to release of nanomolar concentrations of dissolved Fe from ash suspended in

64   seawater, it was observed that low loadings (< 5 mg L^{-1}) of ash were an unusually prolific

65   source of Fe(II) into chilled seawater (up to 1.0 µmol Fe g^{-1}), producing a pulse of Fe(II)

66   typically released mainly during the first minute after addition to seawater. This release

67   would not be detected, either as Fe(II) or dissolved Fe, following standard leaching protocols

68   at room temperature. A pulse of Fe(II) release upon addition of Calbuco ash to seawater made

69   it an unusually efficient dissolved Fe source. The fraction of dissolved Fe released as Fe(II)

70   from Calbuco ash (~18-38%) was roughly comparable to literature values for Fe released

71   into seawater from aerosols collected over the Pacific Ocean following long range

72   atmospheric transport.

1. Introduction

Volcanic ash has long been considered a large, intermittent source of trace metals to the ocean (Frogner et al., 2001; Sarmiento, 1993; Watson, 1997) and its deposition is now deemed a sporadic generally low-macronutrient, high-micronutrient supply mechanism (Ayris and Delmelle, 2012; Jones and Gislason, 2008; Lin et al., 2011). As volcanic ash can be a regionally significant source of allochthonous inorganic material to affected water bodies, volcanic eruptions have the potential to dramatically change light availability, the carbonate system, properties of sinking particles and ecosystem dynamics (Hoffmann et al., 2012; Newcomb and Flagg, 1983; Stewart et al., 2006). Surveys directly underneath the ash plume from the 2010 eruption of Eyjafjallajökull (Iceland) over the North Atlantic found, among other biogeochemical perturbations, high dissolved Fe (dFe) concentrations of up to 10 nM in affected surface seawater (Achterberg et al., 2013) which could potentially result in enhanced primary production. The greatest potential positive effect of ash deposition on marine productivity would generally be expected in high-nitrate, low-chlorophyll (HNLC) areas of the ocean (Hamme et al., 2010; Mélançon et al., 2014), where low Fe concentrations are a major factor limiting primary production (Martin et al., 1990; Moore et al., 2013). Special interest is therefore placed on the ability of volcanic ash to release dFe, and other bio-essential trace metals such as Mn (Achterberg et al., 2013; Browning et al., 2014; Hoffmann et al., 2012), into seawater. In contrast, apart from inducing light limitation, there are several adverse effects of ash deposition on aquatic organisms. These include metal toxicity (Ermolin et al., 2018), particularly under high dust loading (Hoffmann et al., 2012), and the ingestion of ash particles by filter feeders, phagotrophic organisms or fish (Newcomb and Flagg, 1983; Wolinski et al., 2013). Transient shifts to low pH have also been reported in some, but not all, ash leaching experiments and in some freshwater bodies following

intense ash deposition events, suggesting that significant ash deposition on weakly buffered aquatic environments can also impact and perturb their carbonate system (Duggen et al., 2010; Jones and Gislason, 2008; Newcomb and Flagg, 1983). The greatest negative impact of ash on primary producers would therefore be expected closest to the source where the ash loading is highest and in areas where macronutrients or light, rather than trace elements, limit primary production.

In contrast to the 2010 Eyjafjallajökull plume over the North Atlantic, the 2015 ash plume over the region from the Calbuco eruption (northern Patagonia, Chile) was predominantly deposited over an inshore and coastal region (Romero et al., 2016) (Fig. 1). This led to visible high ash loadings in affected surface waters in the weeks after the eruption (Fig. 2), providing a case study for a concentrated ash deposition event in a coastal system; Reloncaví Fjord, which is the northernmost fjord of Patagonia. It receives the direct discharge from three major rivers, creating a highly stratified and productive fjord system in terms of both phytoplankton biomass and aquaculture production of mussels (González et al., 2010; Molinet et al., 2017; Yevenes et al., 2019). Here we combine in situ observations from moored arrays which were fortuitously deployed in Reloncaví Fjord (Vergara-Jara et al., 2019), with satellite-derived chlorophyll data for offshore regions subject to ash deposition, and leaching experiments carried out on ash collected from the fjord region, to investigate the inorganic consequences of ash addition to natural waters. We thereby evaluate the potential positive and negative effects of ash from the 2015 Calbuco eruption on marine phytoplankton~~arine primary production~~ in three geographical regions; Reloncaví Fjord and the areas of the SE Pacific and SW Atlantic Oceans beneath the most intense ash plume.

2. **Materials and methods**

2.1. *Study area*

The Calbuco volcano (Fig. 1) is located in a region with large freshwater reservoirs and in close proximity to Reloncaví Fjord. The predominant bedrock type is andesite (López-Escobar et al., 1995). Reloncaví Fjord is 55 km long and receives freshwater from 3 main rivers, the Puelo, Petrohué, and Cochamó, with mean stream flows of 650 m^3 s^{-1}, 350 m^3 s^{-1} and 100 m^3 s^{-1}, respectively (León-Muñoz et al., 2013). River discharge strongly influences seasonal patterns of primary production across the region, supplying silicic acid and strongly stratifying the water column (Castillo et al., 2016; González et al., 2010; Torres et al., 2014). Seasonal changes in light availability rather than macronutrient supply are thought to control marine primary production across the Reloncaví region with high marine primary production (>1 g C m^{-2} day^{-1}) throughout austral spring, summer and early autumn (González et al., 2010).
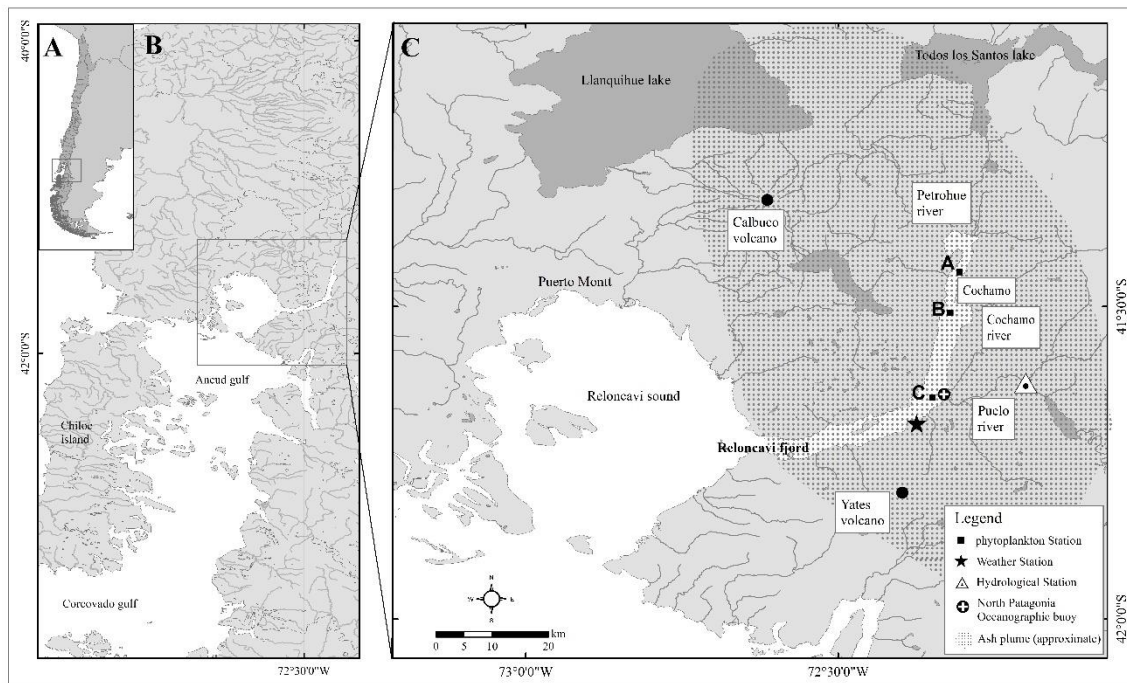
Figure 1. The Calbuco region showing the location of Reloncaví Fjord, 3 major rivers (Petrohué, Cochamó and Puelo) discharging into the fjord, the 3 stations (black squares; A, B and C) used to assess changes in phytoplankton abundance following the eruption, a hydrological station that monitors Puelo river flow, a weather station and the location of a long-term mooring within the fjord. The approximate extent of the ash plume in the week following the first eruption is illustrated, as estimated in technical reports issued by the Servicio Nacional de Geología y Minería (Chile).

On 22 April 2015 the Calbuco volcano erupted after 54 years of dormancy. Two major eruption pulses lasted <2 hours on 22 April and 6 hours on 23 April, releasing a total volume of 0.27 km^3 ash which was projected up to 20 km height above sea level (Van Eaton et al., 2016; Romero et al., 2016). Ash layers of several cm thick were deposited mainly to the NE of the volcano in subsequent days (Romero et al., 2016). A smaller eruption occurred on 30 April projecting ash 4-5 km above sea level which was then mainly deposited south of the volcano. Smaller volumes of ash were released semi-continuously for three weeks after the main eruption, leading to intermittent ash deposition events. Fortuitously, as part of a long-term deployment, an ocean acidification buoy in the middle of Reloncaví Fjord (Vergara-Jara et al., 2019) and an associated meteorological station close to the volcano (Fig. 1) were well placed to assess the impact of ash deposition immediately after the eruption. To complement data from these facilities, after the regional evacuation order was removed, weekly sampling campaigns were conducted in the fjord commencing one week after the eruption. The Chilean Geological-mining Survey (Servicio Nacional de Geología y Minería, SERNAGEOMIN) produced daily technical reports including the estimated area of ash dispersion   (http://sitiohistorico.sernageomin.cl/volcan.php?pagina=4&iId=3).   This

159   information was used to create a reference aerial extent of ash deposition for the week after

160   the eruption (Fig. 1, C). This approximation represents a full week of coverage for this

161   dynamic feature.

162

163   **2.2. Ash samples – trace metal leaching experiments**

164   On 6 May (2015, Cochamó, Chile, approximately 30 km from the volcano) after the third,

165   and smallest, eruptive pulse of ash from the Calbuco volcano (Fig. 2, A), and with the volcano

166   still emitting material, ash was collected using a plastic tray wrapped with plastic sheeting

167   (40×94 cm). The plasticware was left outside for 24 hours until sufficient ash (~500 g) was

168   collected to provide a bulk sample. Ambient weather over the period of ash collection, and

169   the preceding day, was dry (no precipitation). The collected ash was double sealed in low

170   density polyethylene (LDPE) plastic bags and stored in the dark. A sub-sample was analyzed

171   for particle size using a Mastersizer 2000 at The University of Chile.

172   Ash may affect in situ phytoplankton dynamics in several ways, for example via moderating

173   the carbonate system, macronutrient availability and/or micronutrient availability. As

174   micronutrient (e.g. Fe and Mn) availability is expected to be the main chemical mechanism

175   via which phytoplankton dynamics in the offshore marine environment could be affected, we

176   primarily focus our investigation on the release of dissolved trace metals from ash in

177   seawater. Yet to rule out other potential affects, we also conduct complementary leaches to

178   assess the significance of changes to total alkalinity and macronutrient availability (Table 1).

179   For trace metal leaches, a variety of methods have been used in the literature (Duggen et al.,

180   2010; Witham et al., 2005) depending on the purpose of specific studies. De-ionized water

181   leaches with ash loadings that are high in an offshore environmental context are preferable

182   for intercomparison studies. The trace metals released under such conditions are however

183   difficult to compare quantitatively to metal exchange processes in the ambient marine

184   environment, especially for elements such as Fe where solubility is strongly influenced by

185   pH, salinity and the nature of dissolved organic carbon present (Baker and Croot, 2010). For

186   prior work conducted specifically using volcanic ash in seawater, 3 main methods have been

187   employed: suspension experiments followed by analysis of the leachate, flow-through

188   reactors, and continuous voltammetric determination of dFe concentrations in situ during

189   suspension experiments (Sup. Table 1). The most commonly used ash:solute ratio in prior

190   seawater experiments is 1:400 (g:mL), with leach lengths varying from 15 minutes to 24

191   hours (Sup. Table 1). Conversely, incubation experiments designed to test the response of

192   marine phytoplankton to ash deposition have used lower ash:solute ratios of 1:400 to $1:10^7$

193   which are based on estimates of the ash loading expected to be mixed within the offshore

194   surface mixed layer underneath ash plumes (Browning et al., 2014; Hoffmann et al., 2012).

195   Existing data suggests that ash:solute ratio is not a major factor in determining the release

196   behavior of Fe from ash, however this is acknowledged to be difficult to assess due to other

197   differences between experimental setups used to date (Duggen et al., 2010). Both the age of

198   particles since collection and the organic carbon content of seawater are however known to

199   be critical factors influencing the exchange of Fe, and other trace elements, following any

200   aerosol deposition into seawater (Baker and Croot, 2010; Duggen et al., 2010). Whilst UV-

201   treatment of seawater has been used in some experiments (to remove a large part of any

202   natural organic ligands present, Duggen et al., 2007; Jones and Gislason, 2008), and a strong

203   synthetic organic ligand added in others (to impede dissolved Fe precipitation, Duggen et al.,

204   2007; Olgun et al., 2011; Simonella et al., 2015), to improve reproducibility and

205   standardisation, these steps are not well suited specifically for investigating the release of

9

206   Fe(II) from ash. Herein we therefore adopt ash:solute ratios comparable to the lower end of

207   the range used in leaching experiments and comparable to the range used in incubation

208   experiments. Seawater was used after prolonged storage in the dark (to reduce biological

209   activity to low background levels) and without UV treatment (to maintain an environmentally

210   relevant level of natural organic material in solution). A short leaching time (10 minutes +

211   filtration) was adopted to minimize bottle effects and recognising that most prior work

212   suggests a large fraction of Fe release occurs on short timescales (minutes), followed by more

213   gradual changes on timescales of hours to days (Duggen et al., 2007; Frogner et al., 2001;

214   Jones and Gislason, 2008).

215   A variety of leaches were conducted in de-ionized water, brackish (fjord) water or offshore

216   South Atlantic seawater (Table 1) with the choice of leaching conditions based on the

217   expected environmental significance in different water masses. Offshore oligotrophic

218   seawater for incubation experiments was collected from an underway transect of the mid-

219   South Atlantic (across 40° S) using a towfish and trace metal clean tubing in a 1 m^3 high

220   density polyethylene tank which had been pre-rinsed with 1 M HCl. This water was stored

221   in the dark for >12 months prior to use in leaching experiments and was filtered

222   (AcroPak1000 capsule 0.8/0.2 µm filters) when subsampling a batch for use in all leaching

223   experiments. All labware for trace metal leaching experiments was pre-cleaned with Mucasol

224   and 1 M HCl. 125 ml LDPE bottles (Nalgene) for trace metal leach experiments were pre-

225   cleaned using a 3-stage procedure with three de-ionized water (Milli-Q, Millipore,

226   conductivity 18.2 MΩ cm^{-1}) rinses after each stage (3 days in Mucasol, 1 week in 1 M HCl,

227   1 week in 1 M HNO$_3$).

228   Leach experiments were conducted by adding a pre-weighed mass of ash into 100 ml South

229 Atlantic Seawater, gently mixing the suspension for 10 minutes, and then syringe filtering

230 the suspension (0.2 µm, polyvinylidene fluoride, Millipore). Eight different ash loadings

231 from 2-50 mg L^{-1} were used, selected to be environmentally relevant and comparable to prior

232 incubation experiments, with each treatment run in triplicate. Samples for dissolved trace

233 metals (Fe, Cd, Pb, Ni, Cu, Co and Mn) were acidified within 1 day of collection by the

234 addition of 140 µL concentrated HCl (UPA grade, ROMIL) and analysed by inductively

235 coupled plasma mass spectroscopy following preconcentration exactly as per Rapp et al.,

236 (2017).

237 Leach experiments specifically to measure Fe(II) release were conducted in a similar manner

238 but in cold seawater with continuous in-line analysis (5-7°C see Sup. Table 2) due to the

239 rapid oxidation rate of Fe(II) at room temperature (~21°C), which makes accurate

240 measurement of Fe(II) concentrations challenging (Millero et al., 1987). For these

241 experiments, a pre-weighed mass of ash was added to 250 ml South Atlantic seawater and

242 manually shaken for approximately one minute, using an expanded loading range from 0.2-

243 4000 mg L^{-1}. Fe(II) was measured via flow injection analysis using luminol

244 chemiluminescence (Jones et al., 2013) without pre-concentration or filtration. The inflow

245 line feeding the flow injection apparatus was positioned inside the ash suspension

246 immediately after mixing and measurements begun thereafter at 2 minutes resolution.

247 Reported mean values (± standard deviation) are determined from the Fe(II) concentrations

248 measured 2-30 minutes after adding ash into solution. Calibrations were run daily using

249 standard additions of 0.2-10 nM Fe(II) to aged South Atlantic seawater at the same

250 temperature with integrated peak area used to construct calibration curves. Following each

251 leaching experiment the apparatus was rinsed with 0.1 M HCl (reagent grade) followed by

252 flushing with de-ionized water to ensure the removal of ash particles. Blank measurements

253 before/after Fe(II) measurements from experiments with different ash loadings verified that

254 there was no discernable interference from ash particles in the Fe(II) flow-through

255 measurements. Fe(II) leaches were conducted 2 weeks, 4 months and 9 months after the

256 eruption. Fe(II) leaches 2 weeks after the eruption were run for 30 minutes. Fe(II) leaches

257 after 4 or 9 months were run for 1 hour to further investigate the temporal development of

258 Fe(II) concentration. The trace metal leach experiments (above) were conducted at the same

259 time as the first Fe(II) incubation experiments (2 weeks after ash collection).

260 For trace metal leaches, the initial (mean ± standard deviation) dissolved trace metal

261 concentrations were deducted from the final concentrations, in order to calculate the net

262 change as a result of ash addition. For Fe(II) measurements, background levels of Fe(II) were

263 below detection (<0.1 nM) and so no deduction was made.

264 **2.3 Ash samples – de-ionized and brackish water leaching experiments**

265 Fresh brackish sub-surface water from the Patagonia study region was obtained from the

266 Aysén Fjord, at Ensenada Baja (45º21'S: 72º40'W, salinity 16.3), close to the Coyhaique

267 laboratory (Aysén region, Chile) and free from the influence of ash from the 2015 eruption.

268 The oceanographic conditions in these waters are similar to the adjacent Reloncaví fjord

269 (Cáceres et al., 2002). De-ionized water, along with the Aysén fjord brackish water, were

270 used for leaching experiments using two size fractions of ash following the general

271 recommendations of Duggen et al., (2010) and Witham et al., (2005) to consider the effects

272 of different size fractions and leachates. Leaches were conducted in 50 ml LDPE bottles filled

273 with either 40 ml brackish or DI-water with 4 replicates of each treatment. Bottles were

12

274   incubated inside a mixer at room temperature after the addition of 0.18 g ash, using two ash

275   size fractions (<63 μm and 250-1000 μm) which were separated using sieves (ASTM e-11

276   specification, W.S. Tyler). The mass distribution of the ash as determined by sieving was

277   4.54% >2360 μm; 6.85% <2360 μm and >1000 μm; 31.12% <1000 μm and >250 μm;

278   24.14% <250 μm and >125 μm; 18.04% <125 μm and >63 μm; 15.31% <63 μm. The

279   dominant size fraction by mass was thereby the 250-1000 μm fraction which was analyzed

280   in addition to the finest fraction (<63 μm) with the greatest surface area to mass ratio. The

281   sampling times were at time zero (defined as just after the addition of the ash and a few

282   minutes of mixing), 2 h and 24 h later. Leaching experiments conducted with brackish water

283   were analyzed for total alkalinity (A_T) via a potentiometric titration using reference standards

284   (Haraldsson et al., 1997) ensuring a reproducibility of <2 μmol/kg. For the de-ionized water

285   leaching experiment, A_T was analyzed by titration of unfiltered 5 ml subsamples to a pH 4.5

286   endpoint (Bromocresol Green/Methyl Red) using a Dosimat (Metrohm Inc) and 0.02 N

287   H_2SO_4 titrant. Alkalinity was calculated as $CaCO_3$ equivalents following APHA (American

288   Public Health Association) 2005-Methods 2320 (2320 Alkalinity, titration method).

289   Additional 5 ml subsamples were filtered, stored at 4°C and analyzed within 3 days for major

290   ions (F^-, Cl^-, SO_4^{2-}, NO_3^-, Li^+, Na^+, NH_4^+, K^+, Mg^{2+}, Ca^{2+}) using a DionexTM 5000 Ion

291   Chromatography system with Eluent Generation (APHA). All measurements were then

292   corrected for initial water concentrations prior to ash addition. Saturation indices for species

293   in solution following leaching from <63 μm ash particles were obtained from the MINTEQ

294   3.1. IAP Ion Activity Product chemical equilibrium model (see Sup. Table 6).

295   Table 1. Summary of different leaching experiments and samples.

13

Ash/ particle source	De-ionized water leaches	Brackish (fjord) water	South Atlantic seawater	Numberº of replicates
Calbuco ash, sieved <63 µm	Total alkalinity, ion and macronutrients	Total alkalinity	-	4
Calbuco ash, sieved 250-1000 µm	Total alkalinity, ion and macronutrients	Total alkalinity	-	4
Calbuco ash, unsieved	-	-	Trace metals, Fe(II)	3 for trace elements, 1 time series for Fe(II)

296 **2.4 Environmental data – continuous Reloncaví Fjord monitoring**

297 High temporal resolution (hourly) in situ measurements were taken in the Reloncaví fjord

298 (Fig. 1 C, North Patagonia Oceanographic Buoy) at 3 m depth using SAMI sensors that

299 measured spectrophotometric CO_2 and pH (DeGrandpre et al., 1995; Seidel et al., 2008)

300 (Sunburst Sensors, LLC), and an SBE 37 MicroCAT CTD-ODO (SeaBird Electronics) for

301 temperature, conductivity, depth and dissolved O_2, as per Vergara-Jara et al., (2019). Sensor

302 maintenance and quality control is described by Vergara-Jara et al., (2019). The error in pCO$_2$

303 concentrations is estimated to be at most 5% which arises mainly due to a non-linear sensor

304 response and reduced sensitivity at high pCO$_2$ levels >1500 ppm (DeGrandpre et al., 1999).

305 The SAMI-pH instruments used an accuracy test instead of a calibration procedure (Seidel

306 et al., 2008). With the broad pH and salinity range found in the fjord, pH values are subject

307 to a maximum error of ±0.02 (Mosley et al., 2004).

308 A meteorological station (HOBO-U30, Fig. 1) measured air temperature, solar radiation,

14

309 wind speed and direction, rainfall, and barometric pressure every 5 minutes. Puelo River

310 streamflow was obtained from the Carrera Basilio hydrological station (Fig. 1), run by

311 Dirección General de Aguas de Chile (http://snia.dga.cl/BNAConsultas/reportes).

312 **2.5 Field surveys in Reloncaví Fjord post eruption**

313 During May 2015, weekly field campaigns were undertaken in the Reloncaví Fjord.

314 Phytoplankton samples were collected at 3 depths (1, 5 and 10 m) for taxonomic

315 characterization and abundance determination at 3 stations (A, B and C; Fig. 1) using a 5 L

316 Go-Flo bottle. Samples for cell-counts were stored in clear plastic bottles (300 mL) and

317 preserved in a Lugol iodine solution. From each sample, a 10 mL subsample was placed in a

318 sedimentation chamber and left to settle for 16 hr. The complete chamber bottom was

319 scanned at 200× to enumerate the organisms and the result was expressed as number of

320 phytoplankton cells per L of seawater (Hasle, 1978). Phytoplankton were identified to genus

321 or species level, when possible, and divided into diatoms and dinoflagellates. Samples were

322 analyzed using an Olympus CKX41 inverted phase contrast microscope and the Utermöhl

323 method (Utermöhl, 1958). The phytoplankton community composition was then statistically

324 analyzed in R (RStudio V 1.2.5033) using general linear models in order to find statistically

325 significant differences between dates and group abundances. ~~Phytoplankton samples were~~

326 ~~collected at 3 depths (1 m, 5 m and 10 m) for taxonomic characterization and abundance~~

327 ~~determination at 3 stations (A, B and C; Fig. 1) using a 5 L Go-Flo bottle. Samples were~~

328 ~~analyzed using an Olympus CKX41 inverted phase contrast microscope using a 10 ml~~

329 ~~sedimentation chamber and the Utermöhl method (Utermöhl, 1958). The phytoplankton~~

330 ~~community composition was then statistically analyzed in R (RStudio V 1.2.5033) using~~

331 ~~general linear models in order to find statistically significant differences between dates and~~

15

332 ~~group abundances.~~ Additionally, as part of a long-term monitoring program at station C (Fig.

333 1), chlorophyll-a samples were retained from 6 depths (1, 3, 5, 7, 10 and 15 m) on 6 occasions

334 during March-May 2015. Chlorophyll-a was determined by fluorometry after filtering 250

335 ml of sampled water through GFF filters (Whatman) as per Welschmeyer (1994). Two

336 additional profiles close to Station C were obtained from Yevenes et al., (2019). Integrated

337 chlorophyll-a (mg m^{-2}) and diatom abundance (cells m^{-2}) were determined to 15 m depth.

338 Chlorophyll-a within Reloncaví Fjord is invariably concentrated in the upper ~10 m

339 (González et al., 2010; Yevenes et al., 2019) and thus, for comparison to prior reported data

340 integrated to 10 m, only a small difference is anticipated. For all profiles considered herein,

341 there is a 20% difference between integrating to 10 m or 15 m depth.

342 **2.6 Satellite data**

343 Daily, 4 km resolution chlorophyll-a images from the MODIS Aqua sensor (OCI algorithm;

344 Hu et al., 2012) were downloaded from the NASA Ocean Color website

345 (https://oceancolor.gsfc.nasa.gov) for the period 4 April 2015–2 May 2015. As the UV

346 Aerosol Index largely reflects strongly UV-absorbing (dust) aerosols (Torres et al., 2007),

347 this was used as a proxy for the spatial extent and loading of the ash plume. The UV aerosol

348 index product from the Ozone Monitoring Instrument (OMI) on the EOS-Aura was

349 downloaded for the same time period. Daily images were composited into 5-day mean

350 averages.

351 **3. Results**

352 **3.1 In situ observations**

353 The Calbuco ash plume reached up to 20 km height and was dispersed hundreds of kilometers

354 across Patagonia and the Pacific and Atlantic Oceans (Fig. 2) (Van Eaton et al., 2016;

355 Reckziegel et al., 2016; Romero et al., 2016). The ash loading in water bodies near the cone

356 was visually observed to be high, especially near the Petrohué river catchment that drains

357 into the head of the Reloncaví fjord. This ash loading into the fjord was clearly visible on 6

358 May 2015 when ash samples were collected for leaching experiments (Fig. 2).

359
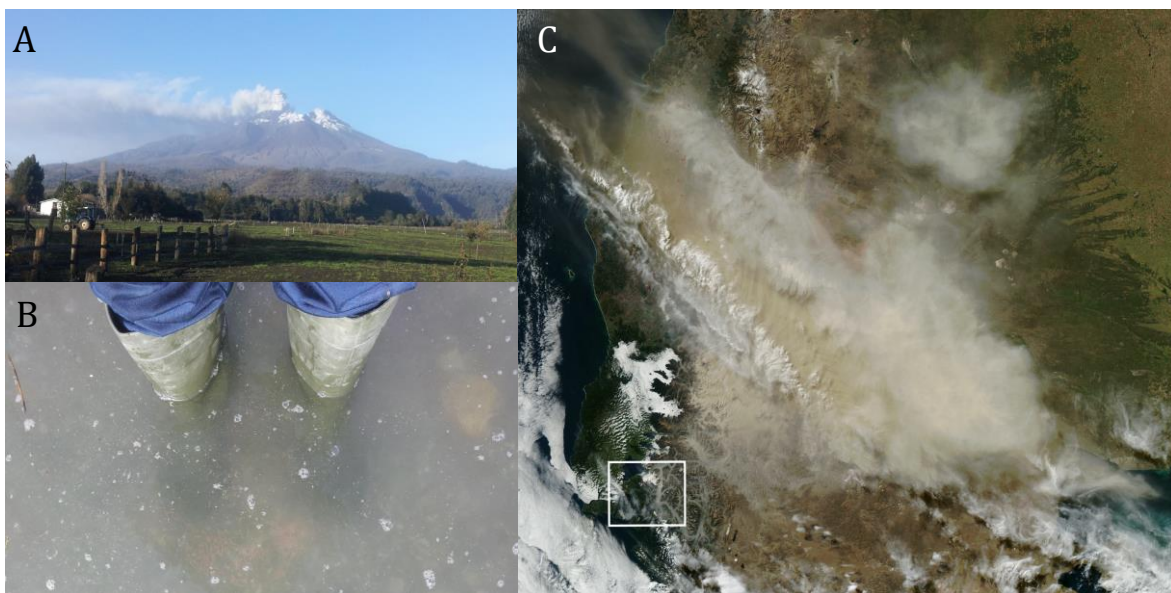
360 Figure 2. A Calbuco volcano ash plume 6 May 2015. B Reloncaví Fjord water with atypical

361 high turbidity due to the ash loading, Cochamó town 6 May. C Ash cloud visible on MODIS

362 Aqua satellite from the NASA Earth Observatory, 23 April

363 (http://earthobservatory.nasa.gov/NaturalHazards/view.php?id=85767&eocn=home&eoci=

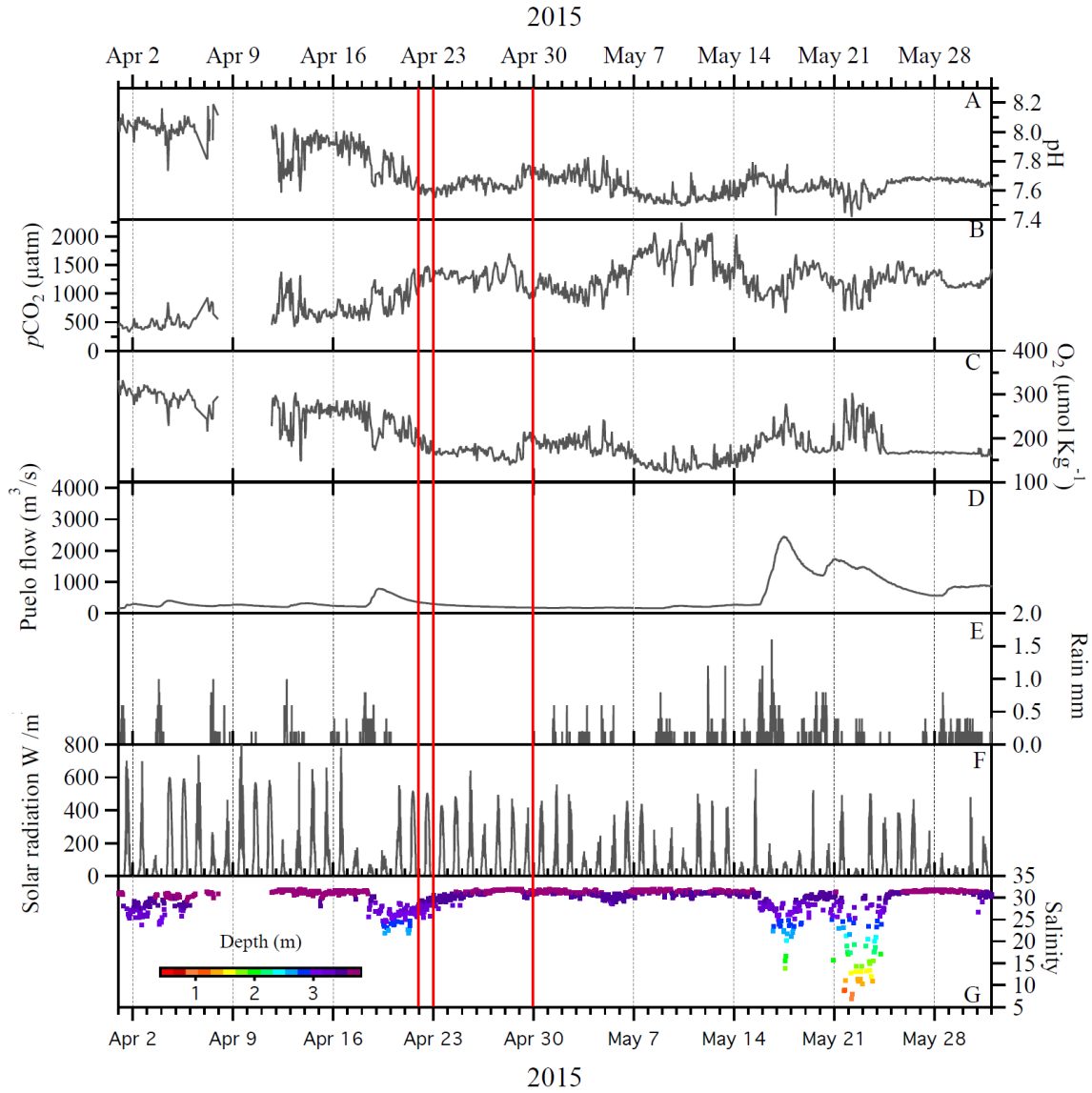364 nh). The highlighted box in C corresponds to Fig. 1 C.

365

Figure 3. Continuous data from the Reloncaví Fjord mooring and nearby hydrological and weather stations for April-May 2015. The vertical red lines mark the eruption dates. All locations are marked in Fig 1. Carbonate chemistry and salinity data from Vergara-Jara et al., (2019). Wind and tidal mixing caused small changes in the depth of the sensors which are shown alongside the salinity data.

371

372 Carbonate chemistry data from the Reloncaví Fjord mooring demonstrated that pH declined

373 and pCO_2 increased in the week prior to the first eruption (22 April, Fig. 3). Oxygen and pH

374 reached a minimum and pCO_2 a maximum during the time period 7-14 May, which indicates

375 a state of high respiration. In this stratified environment, the brackish fjord surface layer has

376 generally low pH, high pCO_2 with seasonal changes in salinity and respiration leading to a

377 large annual range of pCO_2 and pH (Vergara-Jara et al., 2019). The depth of the sensors

378 varied temporally due to changes in tides and river flow. This accounts for some of the

379 variation in measured salinity due to the strong salinity gradient with depth in the brackish

380 surface waters (Fig. 3). Any changes to pCO_2 or pH occurring as a direct result of the

381 eruptions, or associated ash deposition, are therefore challenging to distinguish from

382 background variation due to short-term (intra-day) or seasonal shifts in the carbonate system

383 which are pronounced in this dynamic and strongly freshwater influenced environment (Fig.

384 3). Freshwater discharge from the Puelo increased sharply from 16 May which is an annually

385 recurring event (González et al., 2010).

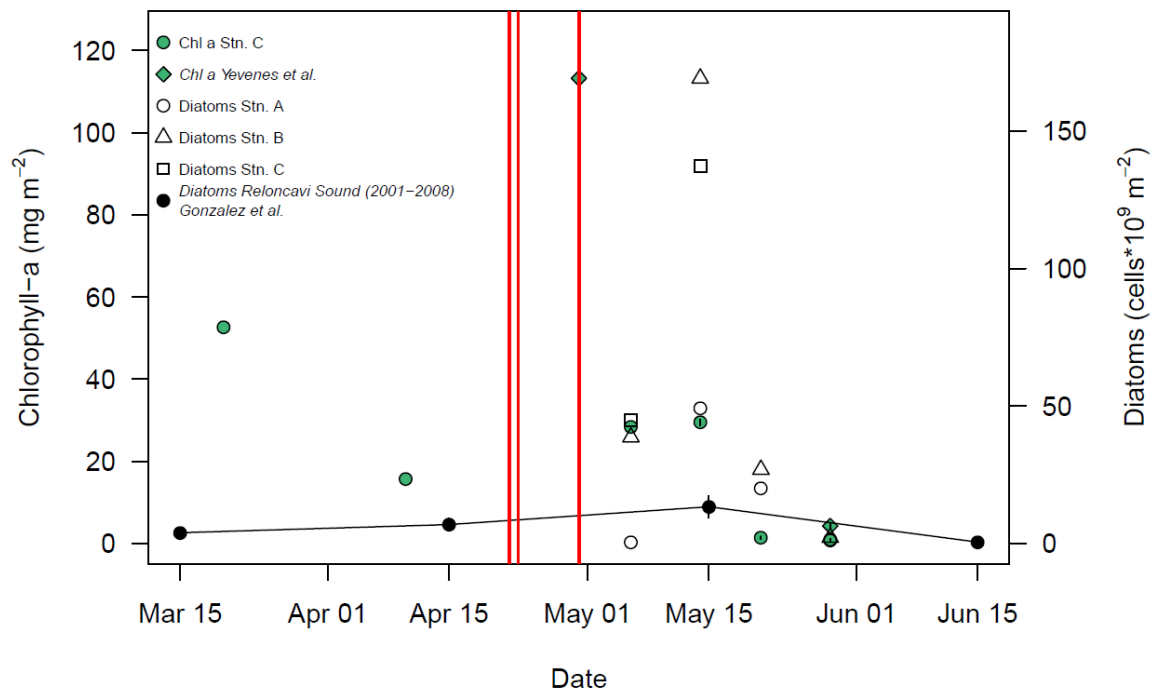386 **3.2 Phytoplankton in Reloncaví fjord post-eruption**

387

Figure 4. Changes in integrated (0-15 m) diatom abundance and chlorophyll-a for Reloncaví

Fjord in April-May 2015. Locations as per Fig. 1, the eruption dates are marked with red

lines. Historical diatom data from Reloncaví Sound (2001-2008, integrated to 10 m depth,

mean ± standard error, González et al., 2010) and additional chlorophyll data from 2015

('Station 3' from Yevenes et al., 2019, approximately corresponding to Station C herein) are

also shown.

394

Phytoplankton abundances observed in May 2015 within Reloncaví Fjord were assessed by

diatom cell counts and chlorophyll-a concentrations (Sup. Table 3) and were proportionate

to, or higher than, those previously observed in the region (Fig. 4). When comparing

observations to prior data from González et al., (2010) it should be noted that there is a slight

depth discrepancy (earlier work was integrated to 10 m depth rather than 15 m herein). Yet

as the phytoplankton bloom is overwhelmingly present within the upper 10 m these data do

401   provide a useful comparison. Diatom abundance integrated to 15 m depth peaked at Stations

402   B and C around 14 May, with notably lower abundances at the innermost station A (Fig. 4).

403   The highest measured chlorophyll-a concentrations were on 30 April at Station C, then

404   chlorophyll-a values declined to much lower concentrations in late May which is expected

405   from patterns in regional primary production (González et al., 2010). No measurements were

406   available for 10-30 April 2015 (Fig. 4) and thus it is not possible to determine the timing of

407   the onset of the austral autumn phytoplankton bloom with respect to the volcanic eruptions

408   from the available chlorophyll-a or diatom data. Within this time period, the mooring at

409   Station C (Fig. 3) however did record a modest increase in pH and O_2 from 28-29 April,

410   during a time period when river discharge and salinity were stable, which could be indicative

411   of the autumn phytoplankton bloom onset.

412

413   **3.3 Total alkalinity and macronutrients in leach experiments**

414   Size analysis of the collected ash determined a mean particle diameter of 339 µm. Small ash-

415   particles (<63 µm) resulted in minor, or no significant, changes to A_T in brackish fjord waters

416   (Fig. 5). With larger ash-particles (250-1000 µm) no effect was evident. Conversely, a

417   leaching experiment with de-ionized water showed a small increase in A_T (Fig. 5) for both

418   size fractions. By increasing the A_T of freshwater, ash would act to increase the buffering

419   capacity of river outflow into a typically weak carbonate system like the Reloncaví Fjord

420   (Vergara-Jara et al., 2019). However, the absolute change in A_T was relatively small despite

421   the large ash loading used in all incubations ($< 20\ \mu mol\ kg^{-1}\ A_T$ for ash loading $>4\ g\ L^{-1}$) and

422   therefore it is expected that the direct effect of ash on A_T in situ was limited. Other effects on

423   carbonate chemistry may however arise due to ash moderating the timing and intensity of

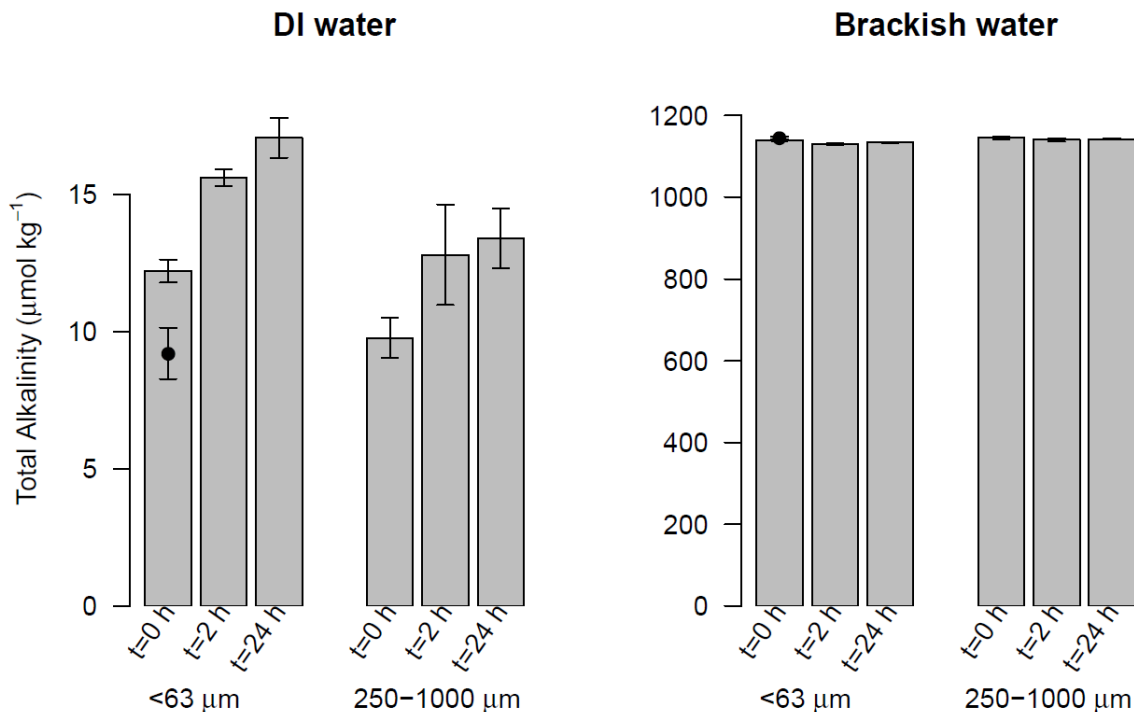424   primary production and thus biological pCO_2 drawdown.

DI water

Brackish water

Figure 5. Total alkalinity released after leaching 4.5 g L^{-1} ash of two size fractions (<63 µm and 250-1000 µm) in de-ionized water (DI water) and brackish water. T$_0$= 'time zero', measured after one minute of mixing, T$_{2H}$= after two hours of mixing, T$_{24H}$= after 24 hours of mixing. n=4 for all treatments (mean ± standard deviation plotted). The initial (pre-ash addition) alkalinity is marked by a black dot superimposed on the left T$_0$. Source data is provided in Supplementary Table 4.

Ion chromatography results for Na$^+$, K$^+$, Ca^{2+}, F$^-$, Cl$^-$, NO$_3^-$ and SO$_4^{2-}$ showed that in the presence of smaller ash size particles, ion inputs were generally higher (Table 2) as has been reported previously (Jones and Gislason, 2008; Óskarsson, 1980; Rubin et al., 1994). The leaching from ash components into de-ionized water occurred almost instantly with limited, or no increases in leached concentrations observed between 0, 2 and 24 h (Table 2). For larger particles there was less release of most ions. In the case of Ca^{2+} and SO$_4^{2-}$ a more gradual

439 leaching effect was apparent (Table 2). The concentrations of NO_3^- and NH_4^+ were generally

440 below detection suggesting that ash was a minor source of fixed-nitrogen into solution. These

441 observations are consistent with the trends in prior work using a range of volcanic ash and

442 incubation conditions (Duggen et al., 2010; Witham et al., 2005). Major ion analysis was

443 only conducted in de-ionized water as no significant changes would be observable for most

444 of these ions in brackish or saline waters under the same conditions.

445

446 Table 2. Major ion and macronutrient concentrations in µmol/l leached from the two size

447 fractions of ash (< 63 µm and 250-1000 µm) into deionized water (b.d. = below detection).

448 Shown are mean values, with the standard deviation in parentheses (n=4). Also shown are

449 mass normalized values [µmol/g ash], and a comparison to the range of values reported by

450 Jones and Gislason (2008).

	Time [h]	**Na$^+$**	**K$^+$**	**Ca^{2+}**	**F$^-$**	**Cl$^-$**	**SO$_4^{2-}$**	**NO$_3^-$**	**NH$_4^+$**
Detection limit		*0.17*	*0.43*	*0.30*	*0.28*	*1.31*	*1.64*	*0.34*	*0.13*
Proced. Blank		b.d.	b.d.	0.39	b.d.	b.d.	b.d.	b.d.	b.d.
250-1000 µm	0.1	3.4 (2.8)	0.83 (0.3)	18.3 (3.3)	0.16 (0.05)	3.7 (1.9)	3.7 (2.2)	b.d.	0.15 (0.2)
[µmol/l]	2	5.1 (2.0)	1.0 (0.2)	18.5 (4.5)	0.21 (0.08)	4.4 (1.6)	4.9 (2.0)	b.d.	0.38 (0.4)
	24	7.3 (0.1)	1.4 (0.2)	23.4 (3.2)	0.52 (0.18)	5.7 (0.5)	8.3 (2.1)	b.d.	b.d.
<63 µm	0.1	16.2 (12.7)	3.2 (0.3)	25.1 (5.4)	0.29 (0.0)	17.1 (13.6)	13.5 (1.3)	0.53 (0.2)	1.70 (1.1)
[µmol/l]	2	16.7 (1.0)	3.8 (0.1)	31.8 (2.7)	0.63 (0.2)	15.2 (0.9)	19.0 (0.3)	b.d.	0.52 (1.0)
	24	17.3 (0.8)	3.9 (0.3)	33.8 (3.3)	0.69 (0.3)	14.6 (1.0)	18.8 (0.5)	b.d.	1.32 (2.6)
<63 µm	24	3.84	0.87	7.50	0.15	3.25	4.18	0.048	0.29
[µmol/g ash]	Range (lit.)	1.5-84.3	0.1-5.4	0.6-589	0.1-9	2-92.9	1-554	0-6.4	0.3-0.6

451

457 **3.4 Trace elements in leach experiments**

458 Release of nanomolar concentrations of dissolved Fe and Mn was evident when ash was re-

459 suspended in aged seawater for 10 minutes (Fig. 6). The net release of dissolved metals

460 proceeded with varying relationships with ash loading over the applied gradient (2-50 mg L$^-$

461 ^{1}). Dissolved Mn, Pb, Cu and Co release exhibited significant ($p < 0.05$) positive relationships

462 with ash loading, with Mn and Cu exhibiting the most linear behavior (R^2 0.99 and 0.83,

463 respectively). Dissolved Fe, Cd and Ni showed no significant relationships with ash loading

464 over the applied range. The initial concentration of metals in South Atlantic seawater should

465 however also be considered when interpreting the trends. The magnitude of changes in Cd

466 and Ni concentrations were smallest relative to both the initial concentration and the standard

467 deviation on the initial concentration (0.38 ± 0.04 nM Cd and 6.58 ± 0.76 nM Ni,

468 respectively). It thus would be difficult to extract a clear relationship irrespective of their

469 chemical behavior. For other elements (Fe, Co and Pb), non-linearity between ash addition

470 and trace metal concentrations, and some negative changes in concentrations, both likely

471 reflect scavenging of metal ions onto ash particle surfaces (Rogan et al., 2016). Fe, Co and

472 Pb are all scavenged type elements and so increasing the surface area of ash present may

473 affect the net change in metal concentration. The divergence between the behaviour of Mn

474 and Fe, with Mn showing a stronger relationship with ash loading, supports the hypothesis

475 of Mendez et al., (2010), that the release of dissolved Mn from aerosols into seawater depends

476 primarily on ash Mn availability whereas the release of dissolved Fe is more dependent on

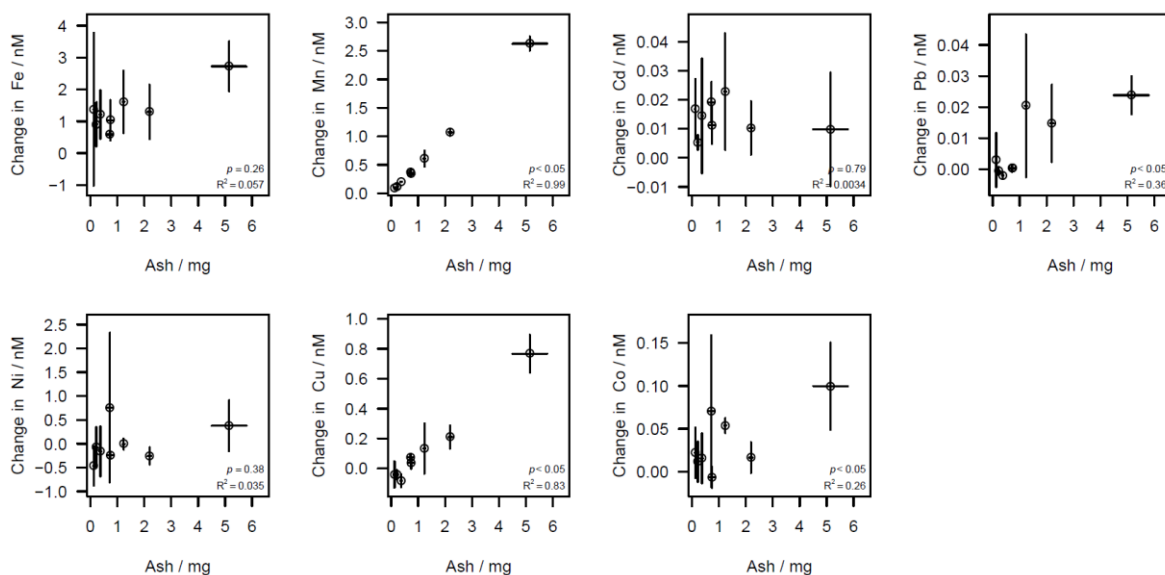477 the nature of organic material present in solution.

478

Figure 6. Change in trace metal concentrations after varying ash addition to 100 ml South Atlantic seawater for a 10-minute leach duration at room temperature. Initial (mean ± standard deviation) dissolved trace metal concentrations - deducted from the final concentrations to calculate the change as a result of ash addition - were 0.98 ± 0.03 nM Fe, 0.38 ± 0.04 nM Cd, 13 ± 2 pM Pb, 6.58 ± 0.76 nM Ni, 0.84 ± 0.07 nM Cu, 145 ± 9 pM Co, 0.72 ± 0.05 nM Mn. Error bars are standard deviations from triplicate treatments with similar ash loadings. p values and R^2 for a linear regression are annotated. Source data is provided in Supplementary Table 5. The same data with individual replicates is shown in Supplementary Figure 1.
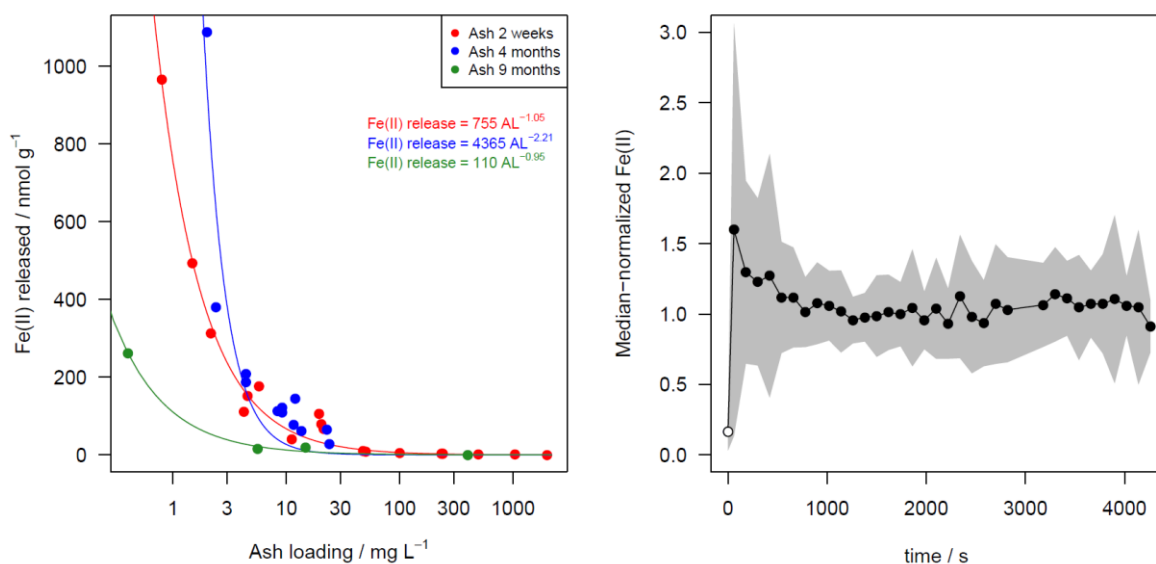
Figure 7. Fe(II) release from Calbuco ash into seawater. Mean Fe(II) released into South Atlantic seawater over a 30 minute leach at 5-7°C (left). The same batch of Calbuco ash was subsampled and used to conduct experiments on 3 occasions after the 2015 eruption (2 weeks, 4 months and 9 months since ash collection). The lines are power law fits, with associated equations shown in the legend. The 3 time-series of Fe(II) concentrations following ash addition is considered collectively by normalizing the measured concentrations (right), such that 1.0 represents the median Fe(II) concentration measured in each experiment. All experiments were conducted for at least 30 minutes, those conducted with 4/9 months old ash were extended for 1 hour. The black line shows the mean response over 34 leach experiments with varying ash loading, the shaded area shows ± 1 standard deviation. The initial Fe(II) concentration (pre-ash addition at 0 s) in all cases was below detection and thus the detection limit is plotted at 0 s (open circle). Source data is provided in Supplementary Table 2.

503   In addition to the release of dFe in solution, which generally exists as Fe(III) species in oxic

504   seawater (Gledhill and Buck, 2012), the release of Fe(II) was evident on a similar timescale

505   when cold (5-7°C) aged S Atlantic seawater was used as leachate (Fig. 7). The half-life of

506   Fe(II) decreases more than tenfold as temperature is increased from 5 to 25°C, leading to

507   Fe(II) decay on timescales shorter than the time required for analysis (approximately 60 s for

508   solution to enter the flow injection apparatus, mix with reagent and generate a peak)

509   (Santana-Casiano et al., 2005). Elevated Fe(II) concentrations (mean 0.8 nM, Sup. Table 2)

510   were evident at this temperature (5-7°C), which represents an intermediate sea surface

511   temperature for the high latitude ocean. A sharp decline in Fe(II) dissolution efficiency with

512   increasing ash load was also evident (Fig. 7). Both the highest Fe(II) concentration and the

513   highest net release of Fe(II) were observed at the lowest ash loading (Fig. 7 and Sup. Fig. 2).

514   Fe(II) concentration following dust addition into seawater was possibly reduced when the

515   same experimental leaches with ash were repeated 9 months after the initial experiment. The

516   first leaches were conducted ~2 weeks after ash collection. The absence of a clear change

517   between 2 weeks and 4 months precludes an accurate assessment of the rate at which Fe(II)

518   solubility may have decreased.

519

520   As Fe(II) concentrations were measured continuously using flow injection analysis, the

521   temporal development of Fe(II) concentration after ash addition to cold seawater can also be

522   shown (Fig. 7). Considering the set of leach experiments collectively, all ash additions were

523   characterized by a sharp increase in Fe(II) concentrations in the first minute after ash addition

524   into seawater. This was typically followed by a decline and then a relatively stable Fe(II)

525   concentration (Fig. 7).

526   **3.5 Satellite observations**

527   Five-day composite images of atmospheric aerosol loading (UV aerosol index, which largely

528   represents strongly UV-absorbing dust, Torres et al., 2007) indicated two main volcanic

529   eruption plume trajectories following the major eruptions on 22 and 23 April: (i) northwards

530   over the Pacific, and (ii) northeast over the Atlantic. Daily resolved time series were

531   constructed for regions in the Atlantic and Pacific with elevated atmospheric aerosol loading

532   (UV Aerosol Index ~2 a.u.; Fig. 8). The Pacific time series indicated a pronounced peak in

533   aerosol index followed by chlorophyll-a one day later. A control region to the south of the

534   ash-impacted Pacific region showed no clear changes in chlorophyll-a matching that

535   observed in the higher UV aerosol index region to the north (Sup. Fig. 3).

536

537   Conversely, in the Atlantic, where the background chlorophyll-a concentration was higher

538   throughout the time period of interest, the main area with enhanced aerosol index was not

539   clearly associated with a change in chlorophyll-a dynamics on a timescale comparable to that

540   observed following other volcanic ash fertilized events (Fig. 8). In a smaller ash impacted

541   area to the south of the Rio de la Plata (Sup. Fig. 3), where nitrate levels are expected to be

542   higher than to the north and Fe levels also expected to be elevated due its location on the

543   continental shelf, a chlorophyll-a peak was evident 7 days after the UV aerosol peak.

544   However, this was not well constrained due to poor satellite coverage in the period after the

545   eruption.

546

547   Prior eruptions have been attributed with driving time periods of enhanced regional marine

548   primary production beginning 3-5 days post-eruption (Hamme et al., 2010; Langmann et al.,

549   2010; Lin et al., 2011) and bottle experiments showing positive chlorophyll changes in

550   response to ash addition are typically significant compared to controls within 1-4 days

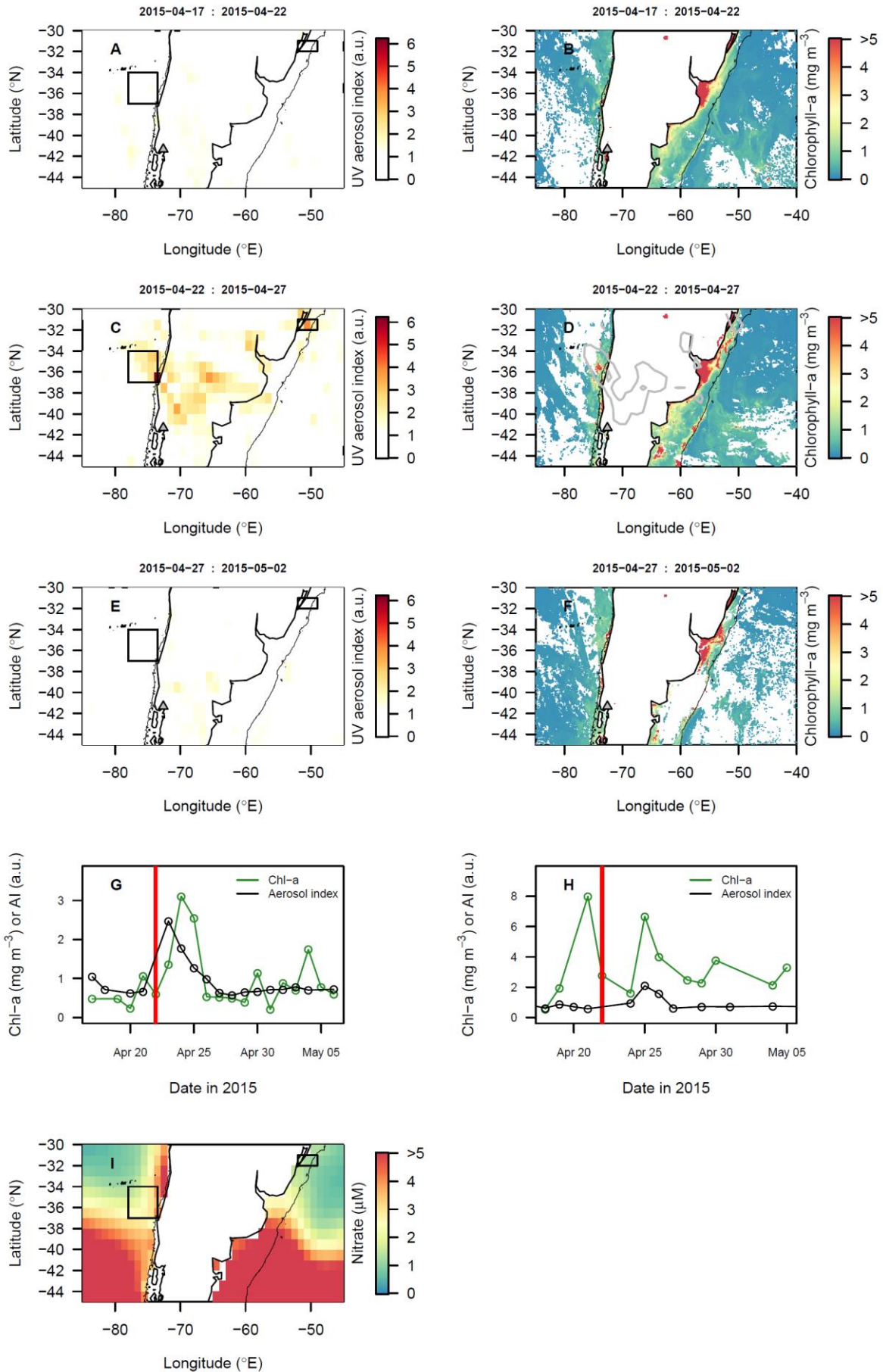551   following ash addition (Browning et al., 2014; Duggen et al., 2007; Mélançon et al., 2014).

553 Figure 8. Potential biological impact of the 2015 Calbuco eruption observed via satellite

554 remote sensing. (A-F) Spatial maps showing the distribution of ash in the atmosphere (UV

555 Aerosol Index) and corresponding images of chlorophyll-a. Images were composited over 5-

556 day periods. Grey lines in chlorophyll maps corresponds to the UV Aerosol index = 2 a.u.

557 contour. (G, H) Time series of UV Aerosol Index and chlorophyll-a for regions of the Pacific

558 (G) and Atlantic (H) identified by boxes in maps. Red vertical lines (22 April) indicate the

559 first eruption date. (I) Mean World Ocean Atlas surface NO_3 concentrations. Thin black lines

560 indicate the 500 m bathymetric depth contour.

561

562 **4 Discussion**

563 **4.1 Local drivers of 2015 bloom dynamics in Reloncaví Fjord**

564 The north Patagonian archipelago and fjord region have a seasonal phytoplankton bloom

565 cycle with peaks in productivity occurring in May and October (austral autumn and spring)

566 and the lowest productivity consistently in June (austral winter)(González et al., 2010).

567 Diatoms normally dominate the phytoplankton community during the productive period due

568 to high light availability and high silicic acid supply, both of which are influenced by

569 freshwater runoff (González et al., 2010; Torres et al., 2014). The austral fall season,

570 encompassing the April-May 2015 ash deposition events, is therefore expected to have a high

571 phytoplankton biomass (Iriarte et al., 2007; León-Muñoz et al., 2018) which terminates

572 abruptly with decreasing light availability in austral winter (González et al., 2010).

573

574 Whilst not directly comparable, the magnitude of the 2015 bloom in terms of diatom

575 abundance (Fig. 4) was more intense than that reported in Reloncaví Sound 2001-2008. With

576 respect to the timing of the phytoplankton bloom, the low diatom abundances and

31

577   chlorophyll-a concentrations at the end of May (Fig. 4) are consistent with prior observations

578   of sharp declines in primary production moving into June (González et al., 2010). Peaks in

579   diatom abundance were measured at two stations on 14 May one week after the third (small)

580   eruptive pulse, and measured chlorophyll-a concentrations were highest close to Station C

581   on 30 April (Fig. 4). The high-resolution pH and O_2 data collected at Station C from mooring

582   data is consistent with an intense phytoplankton bloom between ~29 April and 7 May (Fig.

583   3) indicated by a shift to slightly higher pH and O_2 during this time period when river flow

584   into the fjord was stable.

585

586   Without a direct measure of ash deposition per unit area in the fjord, turbidity, or higher

587   resolution chlorophyll/diatom data, it is challenging to unambiguously determine the extent

588   to which the austral autumn phytoplankton bloom was affected by volcanic activity. The high

589   abundance of diatoms at two of three stations sampled could have resulted from ash

590   fertilization. Yet if this was the case, it is not clear which nutrient was responsible for this

591   fertilization, why the bloom initiation occurred about one week after the third eruptive pulse

592   (several weeks after the main eruption events) and to what extent the timing was coincidental

593   given that productivity normally peaks in May. Reloncaví Fjord was to the south of the

594   dominant ash deposition from the 22 and 23 April eruptions (Romero et al., 2016) and thus

595   ash was delivered by a mixture of vectors including runoff and rainfall. The Petrohue river

596   basin was particularly severely affected by ash with deposition of up to 50 cm ash in places.

597   This complicates the interpretation of the time series provided by high resolution data (Fig.

598   3). With incident light also highly variable over the time series (Fig. 3F), there are clearly

599   several factors, other than volcanic ash deposition, which will have exerted some influence

600   on diatom and chlorophyll-a abundance throughout May 2015.

601

Primary production in the Reloncaví region is thought to be limited by light availability rather

than macronutrient availability (González et al., 2010). Whilst micronutrient availability

relative to phytoplankton demand has not been extensively assessed in this fjord, with such

higher riverine inputs across the region- which are normally a large source of dissolved trace

elements into coastal waters (e.g. Boyle et al., 1977)- limitation of phytoplankton growth by

Fe, or another micronutrient, seems implausible. Reported Fe concentrations determined by

a diffusive gel technique in Reloncaví Fjord in October 2006 were relatively high; 46-530

nM (Ahumada et al., 2011). Similarly, reported dFe concentrations in the adjacent Comau

Fjord at higher salinity are generally in the nanomolar range and remain >2 nM even under

post-bloom conditions which suggests dFe is not a limiting factor for phytoplankton growth

(Hopwood et al., 2020; Sanchez et al., 2019).

Silicic acid availability could have been increased by ash deposition. Whilst not quantified

herein, an increase in silicic acid availability from ash in a region where silicic acid was sub-

optimal for diatom growth could plausibly explain higher than usual diatom abundance

(Siringan et al., 2018). Silicic acid concentrations were indeed high (up to 118 µM) in

Reloncaví Fjord surface waters and >30 µM at 15 m depth (salinity 33.4) (Vergara-Jara et

al., 2019; Yevenes et al., 2019). However concentrations >30 µM are typical during periods

of high runoff and accordingly are not thought to limit primary production or diatom growth

in this area (González et al., 2010). The $Si(OH)_4$:NO_3 ratio in Reloncaví Fjord and

downstream Reloncaví Sound also indicates an excess of $Si(OH)_4$, with ratios of

approximately 2:1 observed in fjord surface waters throughout the year (González et al.,

2010; Yevenes et al., 2019). For comparison, the ratio of Si:N for diatom nutrient uptake is

625   15:16 (Brzezinski, 1985). Furthermore, experimental incubations making additions of

626   macronutrients to fjord waters in Reloncaví and adjacent fjords, have found strong responses

627   of phytoplankton to additions of silicic acid only when $Si(OH)_4$ and NO_3 were added in

628   combination, further corroborating the hypothesis that an excess of silicic acid is normally

629   present in surface waters of these fjord systems (Labbé-Ibáñez et al., 2015). It is therefore

630   doubtful that changes in nutrient availability from ash alone could explain such high diatom

631   abundances in mid-May.

632

633   Alternative reasons for high diatom abundances in the absence of a chemical fertilization

634   effect are plausible and could include, for example, ash having reduced zooplankton

635   abundance or virus activity in the fjord, thus facilitating higher diatom abundance than would

636   otherwise have been observed by decreasing diatom mortality rates in an environment where

637   nutrients were replete. The role of volcanic ash in driving such short-term ecological shifts

638   in the marine environment is almost entirely unstudied (Weinbauer et al., 2017). However,

639   volcanic ash deposition of 7 mg L^{-1} in lakes within this region during the 2011 Puyehue-

640   Cordón Caulle eruption was reported to increase post-deposition phytoplankton biomass and

641   decrease copepod and cladoceran biomass (Wolinski et al., 2013). The proposed mechanism

642   was ash particle ingestion negatively affecting zooplankton, and ash-shading positively

643   affecting phytoplankton via reduced photoinhibition (Balseiro et al., 2014; Wolinski et al.,

644   2013).

645

646   Considering the more modest peak in diatom abundance at the most strongly ash affected

647   station (Station A, Fig. 4) and the timing of the peak diatom abundance 3 weeks after the

648   main eruption, it is clear that the interaction between ash and phytoplankton in the Reloncaví

649   Fjord was more complex than the simple Fe-fertilization proposed for the SE Pacific (Fig.

650   8g). In the absence of an immediate diatom fertilization effect from Fe or silicic acid, we

651   hypothesize that any change in phytoplankton bloom dynamics within Reloncaví Fjord was

652   mainly a 'top-down' effect driven by the physical interaction of ash and different ecological

653   groups in a nutrient replete environment, rather than a 'bottom-up' effect driven by

654   alleviation of nutrient-limitation from ash dissolution.

655   **4.2 Volcanic ash as a unique source of trace elements**

656   The release of the bioessential elements Fe and Mn from ash here ranged from 53 - 1200

657   nmol g^{-1} (dFe) and 48 - 71 nmol g^{-1} (dissolved Mn). For dFe this is comparable to the rates

658   determined in other studies under similar experimental conditions for subduction zone

659   volcanic ash, with reported Fe-release in prior work ranging 2-570 nmol g^{-1} (Sup. Table 1).

660   For Mn, less prior work is available, but these values are within the 17-1300 nmol g^{-1} range

661   reported by Hoffmann et al., (2012). Fe(II) release was particularly efficient at ash loadings

662   <5 mg L^{-1} (Fig. 7), whereas dFe release was less sensitive to ash loading (Fig. 6). The timing

663   of Fe(II) release in the first 60 s of incubations suggests a fast dissolution process. Fe(II) is

664   short lived in oxic surface seawater with an observed half-life of only 10-20 minutes even in

665   the Southern Ocean where cold surface waters slow Fe(II) oxidation (Sarthou et al., 2011).

666   Yet, relative to Fe(III), Fe(II) is also more soluble and, from an energetic perspective,

667   expected to be more bioaccessible to cellular uptake (Sunda et al., 2001). Whilst it is known

668   that the vast majority of dFe leached from ash into seawater tends to occur in the first minutes

669   of ash addition (Duggen et al., 2007; Jones and Gislason, 2008), and this could be consistent

670   with rapid dissolution of highly soluble phases on ash surfaces, we note that there is not yet

671   conclusive evidence concerning the precise origin of this dFe pulse. Fe(II) salts may be

672   present on the surface of ash particles (Horwell et al., 2003; Hoshyaripour et al., 2015) and

673 thus the Fe(II) observed herein (Fig. 7) may reflect almost instantaneous release following

674 dissolution of thin layers of salt coatings in ash surfaces (Ayris and Delmelle, 2012; Delmelle

675 et al., 2007; Olsson et al., 2013). Alternatively Fe(II) could be released from more crystalline

676 Fe(II) phases. Prior work, at much lower pH (pH 1 H_2SO_4 representing conditions that ash

677 surfaces may experience during atmospheric processing, but not in aquatic environments)

678 suggests that short-term release of Fe(II) or Fe(III) is determined by the surface Fe(II)/Fe

679 ratio which may differ from the bulk Fe(II)/Fe ratio due to plume processing (Maters et al.,

680 2017).

681 Different leaching protocols are widely recognised as a major challenge for interpreting and

682 comparing different dissolution experiment datasets for all types of aerosols (Duggen et al.,

683 2007; Morton et al., 2013). When Fe(II) is released into solution as a considerable fraction

684 of the total dFe release this is particularly challenging to monitor, as Fe(II) oxidises on

685 timescales of seconds to minutes depending on temperature, pH and O_2 conditions (Santana-

686 Casiano et al., 2005). The dFe and Fe(II) leaching protocols used herein are only comparable

687 qualitatively, as the Fe(II) method using cooler seawater and larger seawater volumes was

688 specifically designed to test for the presence of rapid Fe(II) release and to evaluate the short-

689 term temporal trend of any such release. Yet, for rough comparative purposes, the Fe(II)

690 released was equivalent to $38 \pm 25\%$ (mean $\pm$ standard deviation) of dFe released at ash

691 loadings from 1-10 mg L^{-1} and $19 \pm 17\%$ of dFe for ash loadings from 10-50 mg L^{-1}. These

692 values are reasonably comparable to the 26% median Fe(II)/dFe fraction measured in Fe

693 released into seawater from aerosols collected across zonal transects of the Pacific Ocean

694 (Buck et al., 2013) suggesting that fresh Calbuco ash is roughly comparable in terms of Fe(II)

695 lability to these environmentally processed aerosols.

696 **4.3 A potential fertilization effect in the SE Pacific**

697   Experiments with ash suspensions have shown that ash loading has a restricted impact on

698   satellite chlorophyll-a retrieval (Browning et al., 2015), therefore offering a means to assess

699   the potential biological impact of the 2015 Calbuco eruption in offshore waters. We found

700   evidence for fertilization of offshore Pacific seawaters in the studied area (Fig. 8). Following

701   the eruption date, mean chlorophyll-a concentrations increased ~2.5 times over a broad

702   region where elevated UV aerosol index was detected (Fig. 8G). Both the timing and location

703   of this chlorophyll-a peak were consistent with ash fertilization, with the peak of elevated

704   chlorophyll-a being located within the core of highest atmospheric aerosol loading, and the

705   peak date occurring one day after the main passage of the atmospheric aerosol plume. A

706   similar phytoplankton response timeframe was reported following ash deposition in the NE

707   Pacific following the August 2008 Kasatochi eruption (Hamme et al., 2010) which was

708   similarly thought to be triggered by relief of Fe-limitation (Langmann et al., 2010). At the

709   same time, a control region to the south of the ash-impacted Pacific region showed no clear

710   changes in chlorophyll-a matching that observed in the higher UV aerosol index region to

711   the north (Sup. Fig. 3).

712

713   In the SW Atlantic, two ash impacted areas are highlighted; one to the north (Fig. 8), and one

714   to the south of the Rio de la Plata (Sup. Fig. 3). Nitrate levels are expected to be higher in the

715   south than to the north, with Fe levels expected to be elevated across both locations as a result

716   of their position on the continental shelf. In the area to the north of the Rio de la Plata (Fig.

717   8), ash deposition indicated by the UV aerosol index did not lead to such a clear

718   corresponding change in chlorophyll-a concentrations (Fig. 8H), although with the available

719   data it is not possible to rule out the possibility of fertilisation completely (e.g., whilst also

720   being proceeded by a larger chlorophyll-a peak on 21 April, there is a peak in chlorophyll-a

721 at 25 April coinciding with elevated UV aerosol index). Phytoplankton growth in this region

722 of the Atlantic is expected to be limited by fixed nitrogen availability, as a result of strong

723 stratification (Moore et al., 2013) and thus dFe release from ash particles alone would not be

724 expected to result in short-term increases to primary production. In the second area of ash

725 deposition, to the south (Sup. Fig. 3), a chlorophyll-a peak was evident 7 days after the UV

726 aerosol peak. However, this was not well constrained due to poor satellite coverage in the

727 period after the eruption. Considering the dynamic spatial and temporal variation in

728 chlorophyll within this coastal area, it is challenging to associate any change in chlorophyll

729 specifically with ash arrival.

730

731 The change in chlorophyll-a observed in the SE Pacific contrasts with results in Reloncaví

732 Fjord where phytoplankton abundances likely peaked much later than the first ash arrival-

733 after 28 April. The fertilized region of the Pacific (Fig. 8) hosts upwelling of deep waters,

734 supplying nutrients in ratios that are deficient in dFe (Bonnet et al., 2008; Torres and

735 Ampuero, 2009). Fe-limitation of phytoplankton growth in this region is therefore

736 anticipated, which could have been temporarily relieved following ash deposition and dFe

737 release (Fig. 6). The differential responses observed in the Pacific and Atlantic are therefore

738 consistent with the anticipated nutrient limitation regimes (Fe-limited and nitrogen-limited,

739 respectively), and the supply of dFe but not fixed N (NO_3 or NH_4) from the Calbuco ash (Fig.

740 6 and Table 2).

741

742 **5 Conclusions**

743 The contrasting effects of volcanic ash on primary producers in Reloncaví Fjord, the SE

744 Pacific and SW Atlantic Oceans support the hypothesis that the response of primary

38

745 producers is dependent on both the ash loading and the resources limiting primary production

746 in a region at a specific time of year. Leach experiments using ash from the 2015 Calbuco

747 eruption demonstrated a small increase in the alkalinity of de-ionized water from fine, but

748 not coarse ash, and no significant addition of fixed nitrogen (quantified as NO_3 and NH_4) into

749 solution. In saline waters, release of dissolved trace metals including Mn, Cu, Co, Pb, Fe and

750 specifically Fe(II) was evident.

751

752 Strong evidence of a broad-scale 'bottom-up' fertilization effect of ash on

753 phytoplankton~~primary production~~ was not found locally within Reloncaví Fjord, although it

754 is possible that the timing and peak diatom abundance of the autumn phytoplankton bloom

755 may have shifted in response to high ash loading in the weeks following the first eruption.

756 High diatom abundances at some stations within the fjord several weeks after the eruption

757 may have arisen from a 'top-down' effect of ash on filter feeders, although the mechanism

758 can only be speculated herein. No clear positive effect of ash deposition on chlorophyll-a

759 was evident in the SW Atlantic, consistent with expected patterns in nutrient deficiency

760 which suggest the region to be nitrogen-limited. However, in offshore waters of the SE

761 Pacific where Fe is anticipated to limit phytoplankton growth, a chlorophyll-a increase was

762 related with maximum ash deposition and we presume that this increase in chlorophyll-a was

763 likely driven by Fe-fertilization.

764

765 **6. Data availability**

766 The complete 2015 time series from the Reloncaví Fjord mooring is available online

767 (https://figshare.com/articles/Puelo_Bouy/7754258). Source data for Figures 4-7 is included

768 in the Supplement.

769

9. Author contributions

MVJ, MH, JLI and EA designed the study. MVJ, IR, MH, RT and BR conducted analytical and field work. TB conducted satellite data analysis. MV, MH and TB wrote the initial manuscript with all authors contributing to its revision.

793

10. References

Achterberg, E. ., Moore, C. M., Henson, S. A., Steigenberger, S., Stohl, A., Eckhardt, S., Avendano, L. C., Cassidy, M., Hembury, D., Klar, J. K., Lucas, M. I., MacEy, A. I., Marsay, C. M. and Ryan-Keogh, T. J.: Natural iron fertilization by the Eyjafjallajokull volcanic eruption, Geophys. Res. Lett., 40(5), 921–926, doi:10.1002/grl.50221, 2013.

Ahumada, R., Rudolph, A., Gonzalez, E., Fones, G., Saldias, G. and Ahumada Rudolph, R.: Dissolved trace metals in the water column of Reloncavi Fjord, Chile, Lat. Am. J. Aquat. Res., 39, 567–574, doi:10.3856/vol39-issue3-fulltext-16, 2011.

Ayris, P. and Delmelle, P.: Volcanic and atmospheric controls on ash iron solubility: A review, Phys. Chem. Earth, doi:10.1016/j.pce.2011.04.013, 2012.

Baker, A. R. and Croot, P. L.: Atmospheric and marine controls on aerosol iron solubility in seawater, Mar. Chem., 120(1–4), 4–13, doi:10.1016/j.marchem.2008.09.003, 2010.

Balseiro, E., Souza, M. S., Olabuenaga, I. S., Wolinski, L., Navarro, M. B., Laspoumaderes, C. and Modenutti, B.: Effect of the Puyehue-Cordon Caulle volcanic complex eruption on crustacean zooplankton of Andean Lakes, Ecol. Austral, 24, 75–82, 2014.

Bonnet, S., Guieu, C., Bruyant, F., Prášil, O., Van Wambeke, F., Raimbault, P., Moutin, T., Grob, C., Gorbunov, M. Y., Zehr, J. P., Masquelier, S. M., Garczarek, L. and Claustre, H.: Nutrient limitation of primary productivity in the Southeast Pacific (BIOSOPE cruise), Biogeosciences, 5(1), 215–225, doi:10.5194/bg-5-215-2008, 2008.

Boyle, E. A., Edmond, J. M. and Sholkovitz, E. R.: Mechanism of iron removal in estuaries, Geochim. Cosmochim. Acta, 41(9), 1313–1324, doi:10.1016/0016-7037(77)90075-8, 1977.

817   Browning, T. J., Bouman, H. A., Henderson, G. M., Mather, T. A., Pyle, D. M., Schlosser,

818   C., Woodward, E. M. S. and Moore, C. M.: Strong responses of Southern Ocean

819   phytoplankton communities to volcanic ash, Geophys. Res. Lett., 41(8), 2851–2857,

820   doi:10.1002/2014GL059364, 2014.

821   Browning, T. J., Stone, K., Bouman, H., Mather, T. A., Pyle, D. M., Moore, M. and

822   Martinez-Vicente, V.: Volcanic ash supply to the surface ocean – remote sensing of

823   biological responses and their wider biogeochemical significance, Front. Mar. Sci., 2,

824   doi:10.3389/fmars.2015.00014, 2015.

825   Brzezinski, M. A.: The Si:C:N ratio of marine diatoms: interspecific variability and the

826   effect of some environmental variables, J. Phycol., 21(3), 347–357, doi:10.1111/j.0022-

827   3646.1985.00347.x, 1985.

828   Buck, C. S., Landing, W. M. and Resing, J.: Pacific Ocean aerosols: Deposition and

829   solubility of iron, aluminum, and other trace elements, Mar. Chem., 157, 117–130,

830   doi:10.1016/j.marchem.2013.09.005, 2013.

831   Cáceres, M., Valle-Levinson, A., Sepúlveda, H. H. and Holderied, K.: Transverse

832   variability of flow and density in a Chilean fjord, in Continental Shelf Research., 2002.

833   Castillo, M. I., Cifuentes, U., Pizarro, O., Djurfeldt, L. and Caceres, M.: Seasonal

834   hydrography and surface outflow in a fjord with a deep sill: The Reloncaví fjord, Chile,

835   Ocean Sci., 12, 533–544, doi:10.5194/os-12-533-2016, 2016.

836   DeGrandpre, M. D., Hammar, T. R., Smith, S. P. and Sayles, F. L.: In situ measurements of

837   seawater pCO_2, Limnol. Oceanogr., 40(5), 969–975, doi:10.4319/lo.1995.40.5.0969, 1995.

838   DeGrandpre, M. D., Baehr, M. M. and Hammar, T. R.: Calibration-free optical chemical

839   sensors, Anal. Chem., 71(6), 1152–1159, doi:10.1021/ac9805955, 1999.

840   Delmelle, P., Lambert, M., Dufrêne, Y., Gerin, P. and Óskarsson, N.: Gas/aerosol-ash

841   interaction in volcanic plumes: New insights from surface analyses of fine ash particles,

842   Earth Planet. Sci. Lett., 259, 159–170, doi:10.1016/j.epsl.2007.04.052, 2007.

843   Duggen, S., Croot, P., Schacht, U. and Hoffmann, L.: Subduction zone volcanic ash can

844   fertilize the surface ocean and stimulate phytoplankton growth: Evidence from

845   biogeochemical experiments and satellite data, Geophys. Res. Lett.,

846   doi:10.1029/2006GL027522, 2007.

847   Duggen, S., Olgun, N., Croot, P., Hoffmann, L., Dietze, H., Delmelle, P. and Teschner, C.:

848   The role of airborne volcanic ash for the surface ocean biogeochemical iron-cycle: a

849   review, Biogeosciences, 7(3), 827–844, doi:10.5194/bg-7-827-2010, 2010.

850   Van Eaton, A. R., Amigo, Á., Bertin, D., Mastin, L. G., Giacosa, R. E., González, J.,

851   Valderrama, O., Fontijn, K. and Behnke, S. A.: Volcanic lightning and plume behavior

852   reveal evolving hazards during the April 2015 eruption of Calbuco volcano, Chile,

853   Geophys. Res. Lett., 43(7), 3563–3571, doi:10.1002/2016GL068076, 2016.

854   Ermolin, M. S., Fedotov, P. S., Malik, N. A. and Karandashev, V. K.: Nanoparticles of

855   volcanic ash as a carrier for toxic elements on the global scale, Chemosphere, 200, 16–22,

856   doi:10.1016/j.chemosphere.2018.02.089, 2018.

857   Frogner, P., Gislason, S. R. and Oskarsson, N.: Fertilizing potential of volcanic ash in

858   ocean surface water, Geology, 29(6), 487–490, doi:10.1130/0091-

859   7613(2001)029<0487:fpovai>2.0.co;2, 2001.

860   Gledhill, M. and Buck, K. N.: The organic complexation of iron in the marine environment:

861   a review, Front. Microbiol., 3, 69, doi:10.3389/fmicb.2012.00069, 2012.

862   González, H. E., Calderón, M. J., Castro, L., Clement, A., Cuevas, L. A., Daneri, G., Iriarte,

863   J. L., Lizárraga, L., Martínez, R., Menschel, E., Silva, N., Carrasco, C., Valenzuela, C.,

864   Vargas, C. A. and Molinet, C.: Primary production and plankton dynamics in the Reloncaví

865   Fjord and the Interior Sea of Chiloé, Northern Patagonia, Chile, Mar. Ecol. Prog. Ser., 402,

866   13–30, 2010.

867   Hamme, R. C., Webley, P. W., Crawford, W. R., Whitney, F. A., Degrandpre, M. D.,

868   Emerson, S. R., Eriksen, C. C., Giesbrecht, K. E., Gower, J. F. R., Kavanaugh, M. T., Pea,

869   M. A., Sabine, C. L., Batten, S. D., Coogan, L. A., Grundle, D. S. and Lockwood, D.:

870   Volcanic ash fuels anomalous plankton bloom in subarctic northeast Pacific, Geophys. Res.

871   Lett., 37(19), L19604, doi:10.1029/2010GL044629, 2010.

872   Haraldsson, C., Anderson, L. G., Hassellöv, M., Hulth, S. and Olsson, K.: Rapid, high-

873   precision potentiometric titration of alkalinity in ocean and sediment pore waters, Deep Sea

874   Res. Part I Oceanogr. Res. Pap., 44(12), 2031–2044, doi:10.1016/S0967-0637(97)00088-5,

875   1997.

876   Hasle, G. R.: The inverted-microscope method, in Phytoplankton manual., 1978.

877   Hoffmann, L. J., Breitbarth, E., Ardelan, M. V., Duggen, S., Olgun, N., Hassellöv, M. and

878   Wängberg, S.-Å.: Influence of trace metal release from volcanic ash on growth of

879   Thalassiosira pseudonana and Emiliania huxleyi, Mar. Chem., 132–133, 28–33,

880   doi:10.1016/j.marchem.2012.02.003, 2012.

881   Hopwood, M. J., Santana-González, C., Gallego-Urrea, J., Sanchez, N., Achterberg, E. P.,

882   Ardelan, M. V., Gledhill, M., González-Dávila, M., Hoffmann, L., Leiknes, Ø., Magdalena

883   Santana-Casiano, J., Tsagaraki, T. M. and Turner, D.: Fe(II) stability in coastal seawater

884   during experiments in Patagonia, Svalbard, and Gran Canaria, Biogeosciences,

885   doi:10.5194/bg-17-1327-2020, 2020.

886   Horwell, C. J., Fenoglio, I., Vala Ragnarsdottir, K., Sparks, R. S. J. and Fubini, B.: Surface

887   reactivity of volcanic ash from the eruption of Soufrière Hills volcano, Montserrat, West

888   Indies with implications for health hazards, Environ. Res., 93(2), 202–215,

889 doi:10.1016/S0013-9351(03)00044-6, 2003.

890 Hoshyaripour, G. A., Hort, M. and Langmann, B.: Ash iron mobilization through

891 physicochemical processing in volcanic eruption plumes: A numerical modeling approach,

892 Atmos. Chem. Phys., 15, 9361–9379, doi:10.5194/acp-15-9361-2015, 2015.

893 Hu, C., Lee, Z. and Franz, B.: Chlorophyll aalgorithms for oligotrophic oceans: A novel

894 approach based on three-band reflectance difference, J. Geophys. Res. Ocean., 117(C1),

895 doi:10.1029/2011JC007395, 2012.

896 Iriarte, J. L., González, H. E., Liu, K. K., Rivas, C. and Valenzuela, C.: Spatial and

897 temporal variability of chlorophyll and primary productivity in surface waters of southern

898 Chile (41.5–43° S), Estuar. Coast. Shelf Sci., 74(3), 471–480,

899 doi:10.1016/j.ecss.2007.05.015, 2007.

900 Jones, M. R., Nightingale, P. D., Turner, S. M. and Liss, P. S.: Adaptation of a load-inject

901 valve for a flow injection chemiluminescence system enabling dual-reagent injection

902 enhances understanding of environmental Fenton chemistry, Anal. Chim. Acta, 796, 55–60,

903 doi:10.1016/j.aca.2013.08.003, 2013.

904 Jones, M. T. and Gislason, S. R.: Rapid releases of metal salts and nutrients following the

905 deposition of volcanic ash into aqueous environments, Geochim. Cosmochim. Acta, 72(15),

906 3661–3680, doi:10.1016/j.gca.2008.05.030, 2008.

907 Labbé-Ibáñez, P., Iriarte, J. L. and Pantoja, S.: Respuesta del microfitoplancton a la adición

908 de nitrato y ácido silícico en fiordos de la Patagonia chilena, Lat. Am. J. Aquat. Res., 43(1),

909 80–93, doi:10.3856/vol43-issue1-fulltext-8, 2015.

910 Langmann, B., Zakšek, K., Hort, M. and Duggen, S.: Volcanic ash as fertiliser for the

911 surface ocean, Atmos. Chem. Phys., 10, 3891–3899, doi:10.5194/acp-10-3891-2010, 2010.

912 León-Muñoz, J., Marcé, R. and Iriarte, J. L.: Influence of hydrological regime of an Andean

913   river on salinity, temperature and oxygen in a Patagonia fjord, Chile, New Zeal. J. Mar.

914   Freshw. Res., 47(4), 515–528, doi:10.1080/00288330.2013.802700, 2013.

915   León-Muñoz, J., Urbina, M. A., Garreaud, R. and Iriarte, J. L.: Hydroclimatic conditions

916   trigger record harmful algal bloom in western Patagonia (summer 2016), Sci. Rep., 8(1),

917   1330, doi:10.1038/s41598-018-19461-4, 2018.

918   Lin, I. I., Hu, C., Li, Y. H., Ho, T. Y., Fischer, T. P., Wong, G. T. F., Wu, J., Huang, C. W.,

919   Chu, D. A., Ko, D. S. and Chen, J. P.: Fertilization potential of volcanic dust in the low-

920   nutrient low-chlorophyll western North Pacific subtropical gyre: Satellite evidence and

921   laboratory study, Global Biogeochem. Cycles, 25, GB1006, doi:10.1029/2009GB003758,

922   2011.

923   López-Escobar, L., Parada, M. A., Hickey-Vargas, R., Frey, F. A., Kempton, P. D. and

924   Moreno, H.: Calbuco Volcano and minor eruptive centers distributed along the Liquiñe-

925   Ofqui Fault Zone, Chile (41°–42° S): contrasting origin of andesitic and basaltic magma in

926   the Southern Volcanic Zone of the Andes, Contrib. to Mineral. Petrol., 119(4), 345–361,

927   doi:10.1007/BF00286934, 1995.

928   Martin, J. H., Fitzwater, S. E. and Gordon, R. M.: Iron deficiency limits phytoplankton

929   growth in Antarctic waters, Global Biogeochem. Cycles, 4(1), 5–12, 1990.

930   Maters, E. C., Delmelle, P. and Gunnlaugsson, H. P.: Controls on iron mobilisation from

931   volcanic ash at low pH: Insights from dissolution experiments and Mössbauer

932   spectroscopy, Chem. Geol., 449, 73–81, doi:10.1016/j.chemgeo.2016.11.036, 2017.

933   Mélançon, J., Levasseur, M., Lizotte, M., Delmelle, P., Cullen, J., Hamme, R. C., Peña, A.,

934   Simpson, K. G., Scarratt, M., Tremblay, J. É., Zhou, J., Johnson, K., Sutherland, N.,

935   Arychuk, M., Nemcek, N. and Robert, M.: Early response of the northeast subarctic Pacific

936   plankton assemblage to volcanic ash fertilization, Limnol. Oceanogr., 59,

937   doi:10.4319/lo.2014.59.1.0055, 2014.

938   Mendez, J., Guieu, C. and Adkins, J.: Atmospheric input of manganese and iron to the

939   ocean: Seawater dissolution experiments with Saharan and North American dusts, Mar.

940   Chem., 120(1), 34–43, doi:10.1016/j.marchem.2008.08.006, 2010.

941   Millero, F. J., Sotolongo, S. and Izaguirre, M.: The oxidation-kinetics of Fe(II) in seawater,

942   Geochim. Cosmochim. Acta, 51(4), 793–801, doi:10.1016/0016-7037(87)90093-7, 1987.

943   Molinet, C., Díaz, M., Marín, S. L., Astorga, M. P., Ojeda, M., Cares, L. and Asencio, E.:

944   Relation of mussel spatfall on natural and artificial substrates: Analysis of ecological

945   implications ensuring long-term success and sustainability for mussel farming,

946   Aquaculture, 467, 211–218, doi:10.1016/j.aquaculture.2016.09.019, 2017.

947   Moore, C. M., Mills, M. M., Arrigo, K. R., Berman-Frank, I., Bopp, L., Boyd, P. W.,

948   Galbraith, E. D., Geider, R. J., Guieu, C., Jaccard, S. L., Jickells, T. D., La Roche, J.,

949   Lenton, T. M., Mahowald, N. M., Marañón, E., Marinov, I., Moore, J. K., Nakatsuka, T.,

950   Oschlies, A., Saito, M. A., Thingstad, T. F., Tsuda, A. and Ulloa, O.: Processes and

951   patterns of oceanic nutrient limitation, Nat. Geosci., doi:10.1038/ngeo1765, 2013.

952   Morton, P. L., Landing, W. M., Hsu, S. C., Milne, A., Aguilar-Islas, A. M., Baker, A. R.,

953   Bowie, A. R., Buck, C. S., Gao, Y., Gichuki, S., Hastings, M. G., Hatta, M., Johansen, A.

954   M., Losno, R., Mead, C., Patey, M. D., Swarr, G., Vandermark, A. and Zamora, L. M.:

955   Methods for the sampling and analysis of marine aerosols: Results from the 2008

956   GEOTRACES aerosol intercalibration experiment, Limnol. Oceanogr. Methods, 11,

957   doi:10.4319/lom.2013.11.62, 2013.

958   Mosley, L. M., Husheer, S. L. G. and Hunter, K. A.: Spectrophotometric pH measurement

959   in estuaries using thymol blue and m-cresol purple, Mar. Chem., 91, 175–186,

960   doi:10.1016/j.marchem.2004.06.008, 2004.

961 Newcomb, T. W. and Flagg, T. A.: Some effects of Mt. St. Helens volcanic ash on juvenile

962 salmon smolts., Mar. Fish. Rev., 45(2), 8–12, 1983.

963 Olgun, N., Duggen, S., Croot, P. L., Delmelle, P., Dietze, H., Schacht, U., Óskarsson, N.,

964 Siebe, C., Auer, A. and Garbe-Schönberg, D.: Surface ocean iron fertilization: The role of

965 airborne volcanic ash from subduction zone and hot spot volcanoes and related iron fluxes

966 into the Pacific Ocean, Global Biogeochem. Cycles, 25(4), doi:10.1029/2009GB003761,

967 2011.

968 Olsson, J., Stipp, S. L. S., Dalby, K. N. and Gislason, S. R.: Rapid release of metal salts and

969 nutrients from the 2011 Grímsvötn, Iceland volcanic ash, Geochim. Cosmochim. Acta,

970 doi:10.1016/j.gca.2013.09.009, 2013.

971 Óskarsson, N.: The interaction between volcanic gases and tephra: Fluorine adhering to

972 tephra of the 1970 hekla eruption, J. Volcanol. Geotherm. Res., doi:10.1016/0377-

973 0273(80)90107-9, 1980.

974 Rapp, I., Schlosser, C., Rusiecka, D., Gledhill, M. and Achterberg, E. P.: Automated

975 preconcentration of Fe, Zn, Cu, Ni, Cd, Pb, Co, and Mn in seawater with analysis using

976 high-resolution sector field inductively-coupled plasma mass spectrometry, Anal. Chim.

977 Acta, 976, 1–13, doi:10.1016/j.aca.2017.05.008, 2017.

978 Reckziegel, F., Bustos, E., Mingari, L., Báez, W., Villarosa, G., Folch, A., Collini, E.,

979 Viramonte, J., Romero, J. and Osores, S.: Forecasting volcanic ash dispersal and coeval

980 resuspension during the April-May 2015 Calbuco eruption, J. Volcanol. Geotherm. Res.,

981 doi:10.1016/j.jvolgeores.2016.04.033, 2016.

982 Rogan, N., Achterberg, E. P., Le Moigne, F. A. C., Marsay, C. M., Tagliabue, A. and

983 Williams, R. G.: Volcanic ash as an oceanic iron source and sink, Geophys. Res. Lett.,

984 43(6), 2732–2740, doi:10.1002/2016GL067905, 2016.

985 Romero, J. E., Morgavi, D., Arzilli, F., Daga, R., Caselli, A., Reckziegel, F., Viramonte, J.,

986 Díaz-Alvarado, J., Polacci, M., Burton, M. and Perugini, D.: Eruption dynamics of the 22–

987 23 April 2015 Calbuco Volcano (Southern Chile): Analyses of tephra fall deposits, J.

988 Volcanol. Geotherm. Res., 317, 15–29, doi:10.1016/j.jvolgeores.2016.02.027, 2016.

989 Rubin, C. H., Noji, E. K., Seligman, P. J., Holtz, J. L., Grande, J. and Vittani, F.:

990 Evaluating a fluorosis hazard after a volcanic eruption, Arch. Environ. Health,

991 doi:10.1080/00039896.1994.9954992, 1994.

992 Sanchez, N., Bizsel, N., Iriarte, J. L., Olsen, L. M. and Ardelan, M. V.: Iron cycling in a

993 mesocosm experiment in a north Patagonian fjord: Potential effect of ammonium addition

994 by salmon aquaculture, Estuar. Coast. Shelf Sci., 220, 209–219,

995 doi:10.1016/j.ecss.2019.02.044, 2019.

996 Santana-Casiano, J. M., Gonzaalez-Davila, M. and Millero, F. J.: Oxidation of nanomolar

997 levels of Fe(II) with oxygen in natural waters, Environ. Sci. Technol., 39(7), 2073–2079,

998 doi:10.1021/es049748y, 2005.

999 Sarmiento, J. L.: Atmospheric CO2 stalled, Nature, doi:10.1038/365697a0, 1993.

1000 Sarthou, G., Bucciarelli, E., Chever, F., Hansard, S. P., Gonzalez-Davila, M., Santana-

1001 Casiano, J. M., Planchon, F. and Speich, S.: Labile Fe(II) concentrations in the Atlantic

1002 sector of the Southern Ocean along a transect from the subtropical domain to the Weddell

1003 Sea Gyre, Biogeosciences, 8(9), 2461–2479, doi:10.5194/bg-8-2461-2011, 2011.

1004 Seidel, M. P., DeGrandpre, M. D. and Dickson, A. G.: A sensor for in situ indicator-based

1005 measurements of seawater pH, Mar. Chem., 109(1), 18–28,

1006 doi:10.1016/j.marchem.2007.11.013, 2008.

1007 Simonella, L. E., Palomeque, M. E., Croot, P. L., Stein, A., Kupczewski, M., Rosales, A.,

1008 Montes, M. L., Colombo, F., García, M. G., Villarosa, G. and Gaiero, D. M.: Soluble iron

1009   inputs to the Southern Ocean through recent andesitic to rhyolitic volcanic ash eruptions

1010   from the Patagonian Andes, Global Biogeochem. Cycles, 29(8), 1125–1144,

1011   doi:10.1002/2015GB005177, 2015.

1012   Siringan, F. P., Racasa, E. D. R., David, C. P. C. and Saban, R. C.: Increase in Dissolved

1013   Silica of Rivers Due to a Volcanic Eruption in an Estuarine Bay (Sorsogon Bay,

1014   Philippines), Estuaries and Coasts, 41, 2277–2288, doi:10.1007/s12237-018-0428-1, 2018.

1015   Stewart, C., Johnston, D. M., Leonard, G. S., Horwell, C. J., Thordarson, T. and Cronin, S.

1016   J.: Contamination of water supplies by volcanic ashfall: A literature review and simple

1017   impact modelling, J. Volcanol. Geotherm. Res., 158(3), 296–306,

1018   doi:10.1016/j.jvolgeores.2006.07.002, 2006.

1019   Sunda, W. G., Buffle, J. and Van Leeuwen, H. P.: Bioavailability and Bioaccumulation of

1020   Iron in the Sea, in The Biogeochemistry of Iron in Seawater, vol. 7, edited by D. R. Turner

1021   and K. A. Hunter, pp. 41–84, John Wiley & Sons, Ltd, Chichester., 2001.

1022   Torres, O., Tanskanen, A., Veihelmann, B., Ahn, C., Braak, R., Bhartia, P. K., Veefkind, P.

1023   and Levelt, P.: Aerosols and surface UV products form Ozone Monitoring Instrument

1024   observations: An overview, J. Geophys. Res. Atmos., doi:10.1029/2007JD008809, 2007.

1025   Torres, R. and Ampuero, P.: Strong CO2 outgassing from high nutrient low chlorophyll

1026   coastal waters off central Chile (30°S): The role of dissolved iron, Estuar. Coast. Shelf Sci.,

1027   83(2), 126–132, doi:10.1016/j.ecss.2009.02.030, 2009.

1028   Torres, R., Silva, N., Reid, B. and Frangopulos, M.: Silicic acid enrichment of subantarctic

1029   surface water from continental inputs along the Patagonian archipelago interior sea (41-

1030   56°S), Prog. Oceanogr., 129, 50–61, doi:10.1016/j.pocean.2014.09.008, 2014.

1031   Utermöhl, H.: Zur Vervollkommnung der quantitativen Phytoplankton-Methodik, SIL

1032   Commun. 1953-1996, doi:10.1080/05384680.1958.11904091, 1958.

1033   Vergara-Jara, M. J., DeGrandpre, M. D., Torres, R., Beatty, C. M., Cuevas, L. A., Alarcón,

1034   E. and Iriarte, J. L.: Seasonal Changes in Carbonate Saturation State and Air-Sea CO2

1035   Fluxes During an Annual Cycle in a Stratified-Temperate Fjord (Reloncaví Fjord, Chilean

1036   Patagonia), J. Geophys. Res. Biogeosciences, 124(9), 2851–2865,

1037   doi:10.1029/2019JG005028, 2019.

1038   Watson, A. J.: Volcanic iron, CO2, ocean productivity and climate, Nature,

1039   doi:10.1038/385587b0, 1997.

1040   Weinbauer, M. G., Guinot, B., Migon, C., Malfatti, F. and Mari, X.: Skyfall - neglected

1041   roles of volcano ash and black carbon rich aerosols for microbial plankton in the ocean, J.

1042   Plankton Res., 39(2), 187–198, doi:10.1093/plankt/fbw100, 2017.

1043   Welschmeyer, N. A.: Fluorometric analysis of chlorophyll a in the presence of chlorophyll

1044   b and pheopigments, Limnol. Oceanogr., doi:10.4319/lo.1994.39.8.1985, 1994.

1045   Witham, C. S., Oppenheimer, C. and Horwell, C. J.: Volcanic ash-leachates: a review and

1046   recommendations for sampling methods, J. Volcanol. Geotherm. Res., 141(3), 299–326,

1047   doi:10.1016/j.jvolgeores.2004.11.010, 2005.

1048   Wolinski, L., Laspoumaderes, C., Bastidas Navarro, M., Modenutti, B. and Balseiro, E.:

1049   The susceptibility of cladocerans in North Andean Patagonian lakes to volcanic ashes,

1050   Freshw. Biol., 58, 1878–1888, doi:10.1111/fwb.12176, 2013.

1051   Yevenes, M. A., Lagos, N. A., Farías, L. and Vargas, C. A.: Greenhouse gases, nutrients

1052   and the carbonate system in the Reloncaví Fjord (Northern Chilean Patagonia):

1053   Implications on aquaculture of the mussel, Mytilus chilensis, during an episodic volcanic

1054   eruption, Sci. Total Environ., doi:10.1016/j.scitotenv.2019.03.037, 2019.

1055